

Aggregated functional data model applied on clustering and disaggregation of UK electrical load profiles

Gabriel Franco

University of Campinas (UNICAMP), Campinas, Brazil.

E-mail: gabrielfranco89@gmail.com

Camila P. E. Souza

The University of Western Ontario, London, Canada.

Nancy L. Garcia

University of Campinas (UNICAMP), Campinas, Brazil.

Summary. Understanding electrical energy demand at the consumer level plays an important role in planning the distribution of electrical networks and offering of off-peak tariffs, but observing individual consumption patterns is still expensive. On the other hand, aggregated load curves are normally available at the substation level. The proposed methodology separates substation aggregated loads into estimated mean consumption curves, called typical curves, including information given by explanatory variables. In addition, a model-based clustering approach for substations is proposed based on the similarity of their consumers' typical curves and covariance structures. The methodology is applied to a real substation load monitoring dataset from the United Kingdom and tested in eight simulated scenarios.

1. Introduction

In 2019, electricity accounted for 17% of the United Kingdom's final energy consumption. This proportion has been relatively stable in recent years. Moreover, when stratified by sector, residential consumers account for 30% of electricity demand (see Table 1.1 and Chart 5.4 in DUKES (2020)), and they have a significant influence of peak demand in the early evening and the peak is more pronounced in winter (Hamidi et al., 2009). For example, in Brazil, typical curves for residential consumers have a spike in electricity consumption from 6 pm to 8 pm, due partially to the use of electric showers after the workday (Lenzi et al., 2017). It is also well known that in the UK, there is large power surge for 3 to 5 minutes at the end of the most popular TV shows or sporting events, exactly the time that takes to make a cup of tea. One alternative and efficient strategy to not only reduce the chance of overload but also to maximize the use of existing equipment is to provide cheaper off-peak tariffs, such as Economy 7, with off-peak rate usually running from midnight to 7am, while the more expensive daytime rate covers the rest of the day.

Understanding individual customer consumption behaviour is essential to comprehend electrical energy demand and consequently to take action to reduce substation load, such as educational programs and off-peak tariff policies, or even to consider bigger projects like

new power plants and network distribution redesign. Solutions such as the aggregated data model proposed in this work provide estimated typical curves for each customer type based only on aggregated data and enhance comprehension of the covariance structure to assess data uncertainty. On the other hand, it is not expected that these typical curves will be the same for all times, locations and consumers. As said before, there are explanatory, such as temperature, TV programming, and location, that can improve the inference and clustering of these typical curves.

Increasing network distribution and the rise of smart grids have drawn attention to load profile monitoring (Wang et al., 2015). Multiple articles have been published in the literature proposing clustering techniques to segment customers and reduce variability (Prahastono et al., 2007; Li et al., 2015a; Bouveyron et al., 2018). Efforts are also underway to achieve short-term load forecasting using machine learning (Sousa et al., 2014) and deep learning methods (Shi et al., 2017). Although load profile modeling is an important task to comprehend electrical demand variability, it does not provide information on the customer level like smart meters (D'Oca et al., 2014; Gouveia and Seixas, 2016; De Souza et al., 2017), appliances monitoring (Hart, 1992; Arghira et al., 2012; Adjei et al., 2020) and disaggregation methods (Schirmer et al., 2019).

Several widely used machine learning and regression methods were used to study energy disaggregation such as artificial neural networks (Lin and Tsai, 2015; Hosseini et al., 2017), random forests (Bilski and Winiecki, 2017; Schirmer and Mporas, 2019), Support Vector Machines (Basu et al., 2014; Schirmer et al., 2020), wavelet component analysis (Zhu and Lu, 2014) and K -Nearest-Neighbours (Kim et al., 2014). Reviews and comparisons of multiple statistical methods for energy disaggregation are available in Schirmer et al. (2019).

The family of aggregated data models considered in this work was first proposed by Dias et al. (2009). Using the observed electrical load from energy transformers and their market information, the authors composed a non-parametric model to estimate the typical consumption curve of customers in the city of Campinas, Brazil, using basis function expansion and the sample covariance matrix as the model covariance structure. More sophisticated structures, under the Bayesian paradigm, were proposed to study the transformer load curves (Dias et al., 2013, 2015). Later, considering the market (distribution of customers per type) as random, the aggregated data model could identify errors in energy customer classification (Lenzi et al., 2017).

In this work, a generalization of the aggregated data model described above is proposed. Our novel approach performs the disaggregation task by assuming a Gaussian process with mean functional response as an aggregated linear combination of the market, typical customer curves, and explanatory variables. Additional functional variables are incorporated in the typical curve model to comprehend, for example, the impact of temperature on customer load profile. A model-based clustering approach is also proposed to group energy substations with similar disaggregated curves using a mixture of Gaussian processes (Shi et al., 2005; Shi and Choi, 2011; Tresp, 2001) estimated by the Expectation-Maximization algorithm (Dempster et al., 1977; McLachlan and Krishnan, 2007). Finally, structured covariance functionals are proposed to model load variability and correlation decay over time. To show the strength of our method, we analyzed a dataset from electrical load profiles from several substations

across the UK.

This paper is organized as follows. Section 2 presents the UK electrical dataset which is analysed in Section 4. The proposed methodology is presented in Section 3. Section 5 provides some discussion and conclusion. Further analysis of artificial datasets is available as supplementary material. The code is currently available online as an R package at a GitHub repository (<https://github.com/gabriel franco89/aggrmodel>).

2. UK electrical data

The dataset analyzed in this work is a subset of the data first introduced by Li et al. (2015a) and Li et al. (2015b). The initial data contain information on electrical load profiles observed every 10 minutes across 407 electrical energy substations in the northwest portion of the United Kingdom. Observations were taken from October 28, 2012, to March 30, 2013, for a total of 154 days.

Each substation supplies energy to up to eight types of customers. This eight-customer division dates from the 1990s and is organized as two domestic types, unrestricted and “Economy 7”; two non-domestic types, also unrestricted and “Economy 7”; and four non-domestic classes of maximum-demand customers according to their peak-load factor. This distribution has proven to be inefficient because a small delicatessen and a supermarket can be assigned to the same customer type (Wilks, 2010). The variability of non-domestic groups makes the aggregated data model unsuitable because there is no typical curve that could, for example, represent both a supermarket and a small delicatessen. Hence, to apply the proposed model, a subset of the data, consisting of substations with only two types of domestic customers, was considered, resulting in a dataset with 12 substations and the following two types of customers: unrestricted (C1) and “Economy 7” (C2) domestic customers, with the latter referring to a program with cheaper electrical tariffs during the off-peak period.

Only working days were considered in the dataset to remove the weekend effect on electrical energy consumption because it is possibly different than the domestic routine between Monday and Friday. Also, to avoid variability during the Christmas and New Year holidays, observations from January 3 to March 30, 2013, were used instead.

Temperature measurements were obtained through the API of the World Weather Online Web site (worldweatheronline.com), using the substation primary, generally representing a community or a district in Wales, as the location reference (see Table 1 and Figure 1). The downloaded historical temperature data, however, contain observations only every three hours. Hence, to achieve the same observation frequency of 10 minutes as in the electrical load dataset, temperature data were interpolated via a cubic B-spline fit.

Figure 2a provides a visualization of the electrical load profiles corresponding to the 61 days from January 3 to March 30, 2013, for each one of the 12 substations, coloured according to the temperature scale located above the panel. Figure 2b shows the observed temperature at the five substation primaries for the same 61 days as in Figure 2a. The associated market of each substation, that is, the number of C1 and C2 residences, is displayed in Table 1, which shows that the great majority of the customers are unrestricted domestic customers (C1), dominating more than 90% of the market in 10 of 12 substations, whereas substation

Table 1. Primaries, substation names, substation IDs and number of customers of types C1 and C2.

Primary	Substation	C1	C2
Trowbridge	S1	228	3
	S2	146	5
	S3	151	5
Cyncoed	S4	21	88
	S5	218	7
Ringland Newport	S6	155	17
	S7	194	12
Llantarnam Primary	S8	173	9
	S9	163	12
	S10	158	2
	S11	244	10
Usk	S12	46	23

S4 is the only one with a majority of “Economy 7” domestic customers (C2), representing 80.73% of its market.

Except for S4 and S12, all substations presented a similar pattern. Early morning showed the lowest energy consumption until approximately 9 AM, with apparently homogeneous variance during this period. The period between 10 AM and 4 PM showed the largest variability, probably because this is the period when people tend to leave their houses to work, but some stay at a home office, for example. From 5 PM onward, the variability apparently stabilized again, even at the load peak at 7 PM. However, substations S4 and S12 not only did not follow this pattern, but also were distinct one from the other. Their peaks, at late night in substation S12 and before sunrise in S4, probably occur because of lower tariffs at night, encouraging energy consumption outside daytime. Exceptionally, substation S12 has one-third of its market consisting of customers of type C2, which results in relatively higher loads in early morning compared to substations with a great majority of C1 customers, and more variability before 9 AM.

Figures 2a and 2b show that it may be useful to extend the aggregated model to include temperature as a functional covariate to better explain the variability of electrical load profiles. Indeed, most substations experience temperature fluctuations during the daytime, whereas night periods tend to be more stable. Nonetheless, substation S12 is an exception for the temperature pattern as well; it is the only one that shows higher temperature values both day and night.

The particularity of substation S12 may be explained by its geographic location within the Usk primary, shown in Figure 1. S12 is in the town of Monmouth, in the countryside of Wales, with a population of less than three thousand, and is the smallest of all the primaries. To the southwest is Llantarnam, a community in the suburb of Cwmbran, with a population size slightly larger than four thousand, where substations S8 to S11 are located, all consisting mostly of customers of type C1. Not far away is Ringland, in the city of Newport, where substations S6 and S7 are located, with populations approximately double

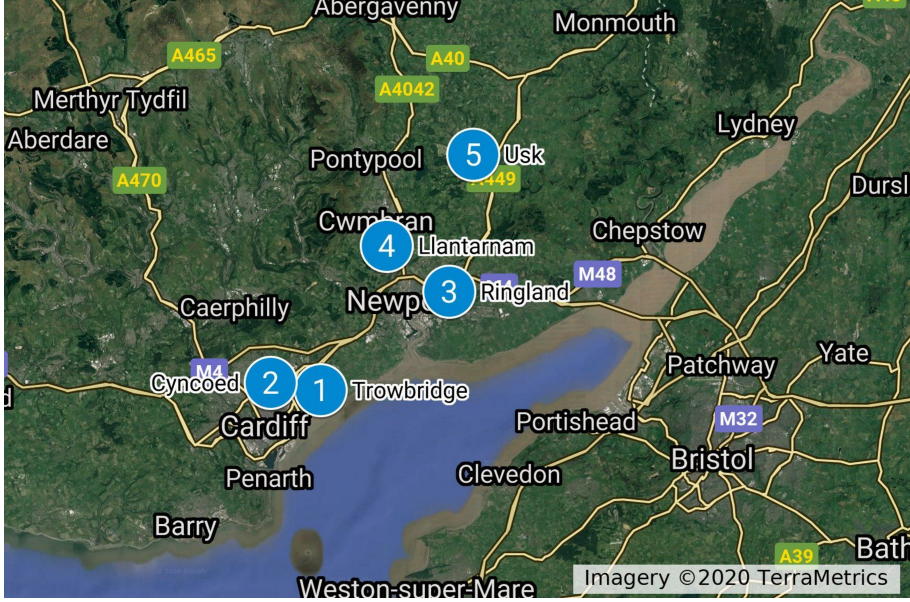


Fig. 1. Geographic location of substation primaries in United Kingdom: (1) Trowbridge, (2) Cyncoed, (3) Ringland, (4) Llantarnam and (5) Usk.

that of Llantarnam. Closer to the capital of Wales, there are two primaries: Trowbridge and Cyncoed. Both are in communities with a population greater than ten thousand (16,194 and 11,148, respectively) located in the urban area of Cardiff Central. In fact, Cyncoed, the only substation with a majority of C2 customers, has some of the highest property prices in the country. All cited demographic data are available in the 2011 census of the United Kingdom for National Statistics (2016).

These different characteristics among substations raise the question if we should assume typical customer curves to be the same for every substation. For example, can it be expected that an unrestricted domestic residence in an urban area like London will have the same load profile as a house located in the countryside? The answer is probably no and this is the motivation to introduce a latent variable to cluster substations based on their disaggregated typical curves and covariance structures.

3. Methods

3.1. Simple aggregated data model

Let us first introduce the aggregated data model in its simplest form, as proposed in Dias et al. (2009). The observed data consist of aggregated energy consumption curves for J substations observed over I days. Each substation constitutes a distinct market with C types of consumers, – e.g., residential, industrial and business. Each aggregated curve is the sum of all individual consumer curves served by that substation. Suppose that $W_{ijcm}(t)$, the

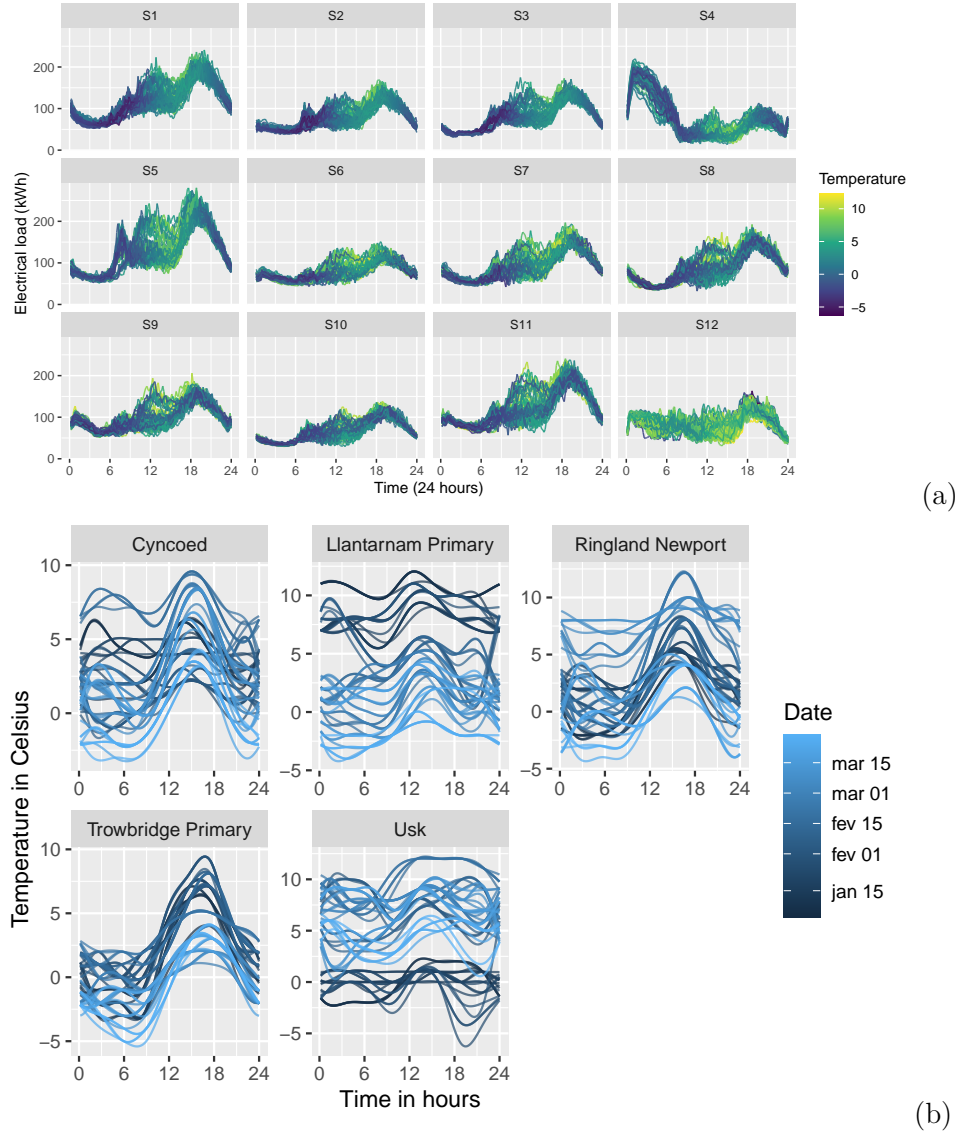


Fig. 2. (a) Electrical load profile data in kWh observed every 10 minutes from 12 substations color-coded by the current air temperature in Celsius and (b) the observed temperature in the five primaries over 61 winter days in the United Kingdom.

unobserved energy consumption of customer m of type c at time t from substation j on day i , can be represented as

$$W_{ijcm}(t) = \alpha_c(t) + \varepsilon_{ijmc}(t), \quad (1)$$

with $\alpha_c(\cdot)$ being the typical curve of a customer of type c and $\varepsilon_{ijmc}(t)$ a Gaussian Process (GP) (Shi and Choi, 2011) with zero mean and covariance structure $\Psi_c(\cdot, \cdot)$ to be detailed in Section 3.3.

Let $Y_{ij}(t)$ be the observable aggregated energy consumption at substation j , day i and time t . $Y_{ij}(t)$ can then be represented as the sum of individual customer curves, that is,

$$\begin{aligned} Y_{ij}(t) &= \sum_{c=1}^C \sum_{m=1}^{m_{jc}} W_{ijcm}(t) \\ &= \sum_{c=1}^C \sum_{m=1}^{m_{jc}} \alpha_c(t) + \varepsilon_{ijmc}(t) \\ &= \sum_{c=1}^C m_{jc} \alpha_c(t) + \varepsilon_{ij}(t), \end{aligned} \quad (2)$$

with m_{jc} being the fixed and known number of customers of type c in substation j , $\varepsilon_{ij}(\cdot, \cdot) \sim GP(0, \Sigma_j(\cdot, \cdot))$, where, assuming independence among individual customers, the covariance structure $\Sigma_j(\cdot, \cdot)$ can be written as $\Sigma_j(s, t) = \sum_{c=1}^C m_{jc} \Psi_c(s, t)$.

The mean component $\alpha_c(\cdot)$ in Equation (1) represents the typical curve of customers of type c and can be modelled using a basis function expansion as $\alpha_c(t) = \sum_{k=1}^K \phi_k(t) \beta_{ck} = \boldsymbol{\phi}(t) \boldsymbol{\beta}_c$, where $\boldsymbol{\beta}_c \in \mathbb{R}^K$ is the vector of expansion parameters or coefficients and $\phi_k(\cdot)$ the k -th basis function, which can be B-Splines, Fourier transforms, wavelets or a polynomial basis (Ramsay and Silverman, 2005). As in previous studies using aggregated data analysis (Dias et al., 2009, 2013, 2015; Lenzi et al., 2017), cubic B-Splines basis are used with the assumption that the number of basis functions K is known. Selection of knot placement and number of basis functions it is an important factor and several studies have dealt with this research topic (DeVore et al., 2003; Dias and Garcia, 2007; Kohn et al., 2000; Luo and Wahba, 1997; Dias, 1998).

3.2. Full aggregated data model

In the electrical energy consumption setup, suppose that the typical curve depends not only on the time t , but also on functional covariates such as the air temperature on day i , $v_i(t)$. Additionally, one can incorporate P explanatory variables related to the substations, namely D_{ij1}, \dots, D_{ijP} to the full aggregated data model in (2), getting

$$Y_{ij}(t) = \left(\sum_{c=1}^C m_{jc} \alpha_c(t, v_i(t)) \right) + D_{ij1} \gamma_1 + \dots + D_{ijP} \gamma_P + \varepsilon_{ij}(t).$$

Again, we will assume that $\alpha_c : \mathbb{R}^+ \times \mathbb{R}$ can be expanded as a tensor product of basis functions as

$$\alpha_c(t, v_i(t)) = \sum_{k=1}^K \sum_{l=1}^L \phi_k(t) \varphi_l(v_i(t)) \beta_{lkc}, \quad (3)$$

where $\phi(\cdot)$ and $\varphi(\cdot)$ are basis functions and β_{lkc} are expansion parameters.

Therefore, we can write the model as

$$Y_{ij}(t) = \left(\sum_{c=1}^C \sum_{k=1}^K \sum_{l=1}^L m_{jc} \phi_k(t) \varphi_l(v_i(t)) \beta_{lkc} \right) + \mathbf{D}_{ij} \boldsymbol{\gamma} + \varepsilon_{ij}(t). \quad (4)$$

In vector representation, $Y_{ij}(t) = \sum_{c=1}^C m_{jc} \boldsymbol{\phi}_i(t) \boldsymbol{\beta}_c + \mathbf{D}_{ij} \boldsymbol{\gamma} + \varepsilon_{ij}(t)$ with $\boldsymbol{\gamma} \in \mathbb{R}^P$ being the parameters corresponding to the substation explanatory variables in \mathbf{D}_{ij} ,

$$\begin{aligned} \boldsymbol{\phi}_i(t) &= \left(\phi_1(t) \varphi_1(v_i(t)), \phi_1(t) \varphi_2(v_i(t)), \dots, \phi_1(t) \varphi_L(v_i(t)), \right. \\ &\quad \left. \phi_2(t) \varphi_1(v_i(t)), \dots, \phi_2(t) \varphi_L(v_i(t)), \dots, \phi_K(t) \varphi_L(v_i(t)) \right) \text{ and} \\ \boldsymbol{\beta}_c &= (\beta_{11c}, \beta_{12c}, \dots, \beta_{1Lc}, \beta_{21c}, \dots, \beta_{2Lc}, \dots, \beta_{KLc}). \end{aligned}$$

Note that the simple model is nested inside the full aggregated data model, because it represents the case when temperature and explanatory variables have no effect on the typical curve.

3.3. Covariance structures

Let $\varepsilon_{ijmc}(\cdot)$ be the Gaussian Process introduced in Equation (1) with zero mean and covariance structure defined by the functional $\Psi_c(\cdot, \cdot)$. This presentation will use the following decomposition (Dias et al., 2013):

$$\Psi_c(s, t) = \text{Cov}(\varepsilon_{ijmc}(s), \varepsilon_{ijmc}(t)) = \eta_c(s) \rho_c(s, t) \eta_c(t),$$

where $\eta_c(\cdot)$ and $\rho_c(\cdot, \cdot)$ are variance and correlation functionals, respectively. To guarantee the positive definiteness of the Gaussian Process covariance structure, $\rho_c(\cdot, \cdot)$ must be a proper positively defined correlation functional. The following sections describe the different nested forms of $\eta_c(\cdot)$ and $\rho_c(\cdot, \cdot)$.

3.3.1. Variance functionals

The variance functional $\eta_c(\cdot)$ describes the variability of customers of type c over time. The identifiability of the model is guaranteed only if $\eta_c(\cdot)$ is positive, otherwise any function multiplied by -1 is also an optimal solution. Hence, the results of Ramsay and Silverman (2005) can be used, and the variance function $\eta_c(\cdot)$ can be written as:

$$\eta_c(\cdot) = \exp \left\{ \sum_{k=1}^{K'} \phi_k^\eta(\cdot) \beta_{kc}^* \right\}. \quad (5)$$

Furthermore, nested functional variances can be created based on a different parametrization of the expansion coefficients of Equation (5) (Dias et al., 2013). If

$$\sigma_c^* = \frac{1}{K'} \sum_{k=1}^{K'} \beta_{kc}^* \quad \text{and} \quad \beta_{kc}^\eta = \beta_{kc}^* - \sigma_c^*,$$

then

$$\eta_c(\cdot) = \exp \left\{ \sigma_c^* + \sum_{k=1}^{K'} \phi_k^\eta(\cdot) \beta_{kc}^\eta \right\}, \quad (6)$$

with $\sum_{k=1}^{K'} \beta_{kc}^\eta = 0$. Now if $\beta_{kc}^\eta = 0, \forall k$, then there is a homogeneous variance $\sigma_c = e^{\sigma_c^*}$ over time for each customer type and if $\sigma_c = \sigma, \forall c$ we have an uniform homogeneity for all types of customer. Hence, the three forms of nested variance functionals are

- (a) Homogeneous uniform: $\eta_c(t) = \sigma, \forall c$;
- (b) Homogeneous: $\eta_c(t) = \sigma_c$;
- (c) Complete: $\eta_c(\cdot) = \sigma_c \exp \left\{ \sum_{k=1}^{K'} \phi_k^\eta(\cdot) \beta_{kc}^\eta \right\}$.

3.3.2. Correlation functional

The correlation functional $\rho_c(s, t)$ quantifies the relationship between the energy consumption of a customer of type c at two points in time s and t in the time interval $[0, T]$. It is assumed that this relationship is defined by an exponential decay proportional to the absolute difference $|t - s|$ and with parameter $\omega_c > 0, \forall c$, that is,

$$\rho_c(s, t) = \exp \left\{ -2 \frac{1}{\omega_c} \frac{|t - s|}{T} \right\}.$$

3.4. Aggregated model likelihood and estimation

The full aggregated data model in Equation (4) includes an error $\varepsilon_{ij}(\cdot)$, which is a Gaussian Process with zero mean and covariance $\Sigma_j(\cdot, \cdot)$. Therefore, we can write $Y_{ij}(\cdot) \sim GP(\mu_{ij}(\cdot), \Sigma_j(\cdot, \cdot))$ with

$$\begin{aligned} \mu_{ij}(t) &= \sum_{c=1}^C m_{jc} \phi_i(t) \beta_c + \mathbf{D}_j \boldsymbol{\gamma} \quad \text{and} \\ \Sigma_j(s, t) &= \sum_{c=1}^C m_{jc} \eta_c(s) \rho_c(s, t) \eta_c(t). \end{aligned} \quad (7)$$

Let \mathbf{y} be a sample of N daily observations from J substations over I days, say

$$\mathbf{y} = \left\{ \mathbf{y}_{ij} : \mathbf{y}_{ij} = (y_{ij}(t_1), \dots, y_{ij}(t_N)) \text{ with } i = 1, \dots, I \text{ and } j = 1, \dots, J \right\}. \quad (8)$$

Note that \mathbf{y} can be made up of substations observed on different days at different time frequencies. However, to simplify the notation it is assumed that all data are observed on the same days and at the same time frequency. Let Θ be the set containing all model parameters. Assuming independence among days and substations, the log-likelihood of the aggregated data model can be written as

$$\begin{aligned}\ell(\Theta|\mathbf{y}) &\equiv \sum_{i=1}^I \sum_{j=1}^J \log f(\mathbf{y}_{ij}; \Theta) \\ &= -\frac{1}{2} \sum_{i=1}^I \sum_{j=1}^J [\log |\Sigma_j| + (\boldsymbol{\mu}_{ij} - \mathbf{y}_{ij})^\top \Sigma_j^{-1} (\boldsymbol{\mu}_{ij} - \mathbf{y}_{ij})] + C,\end{aligned}\quad (9)$$

where

$$\begin{aligned}\boldsymbol{\mu}_{ij} &= \{\mu_{ij}(t_1), \dots, \mu_{ij}(t_N)\} \quad \text{and} \\ \Sigma_j &= \{\Sigma_j \in \mathbb{R}^{N \times N} \text{ with elements } \Sigma_j(s, t) : s = t_1, \dots, t_N; t = t_1, \dots, t_N; \}.\end{aligned}$$

To facilitate parameter estimation, the mean function $\mu_{ij}(\cdot)$ in Equation (7) is written as

$$\mu_{ij}(t) = \mathbf{X}_{ij}(t)\boldsymbol{\beta},$$

where $X_{ij}(\cdot)$ is a matrix composed of the basis functions multiplied by its respective market m_{jc} and the covariates \mathbf{D}_j , that is,

$$\mathbf{X}_{ij}(t) = (m_{j1}\phi_i(t) \quad m_{j2}\phi_i(t) \quad \cdots \quad m_{jC}\phi_i(t) \quad \mathbf{D}_j)_{1 \times (KLC+P)},$$

and $\boldsymbol{\beta} = (\beta_1 \quad \beta_2 \quad \cdots \quad \beta_C \quad \boldsymbol{\gamma})_{1 \times (KLC+P)}$ is made up of the parameters of the basis expansion and the coefficients of the explanatory variables. With this vector representation, we can write the aggregated data model as

$$\mathbf{Y}_{ij} = \mathbf{X}_{ij}\boldsymbol{\beta} + \boldsymbol{\varepsilon}_{ij},$$

where $\mathbf{X}_{ij}^T = [\mathbf{X}_{ij}(t_1) \cdots \mathbf{X}_{ij}(t_N)]_{(KLC+P) \times N}$ and $\boldsymbol{\varepsilon}_{ij} = (\varepsilon_{ij}(t_1), \dots, \varepsilon_{ij}(t_N))^T$.

Furthermore, the model can be represented across all J substations over I days using a single vector \mathbf{Y} , that is,

$$\mathbf{Y} = \mathbf{X}\boldsymbol{\beta} + \boldsymbol{\varepsilon},$$

where

$$\begin{aligned}\mathbf{Y}_{(NIJ) \times 1} &= (\mathbf{Y}_{11}, \mathbf{Y}_{21}, \dots, \mathbf{Y}_{I1}, \mathbf{Y}_{12}, \dots, \mathbf{Y}_{IJ})^T, \\ \mathbf{X}_{NIJ \times (KLC+P)} &= (\mathbf{X}_{11}, \dots, \mathbf{X}_{I1}, \mathbf{X}_{12}, \dots, \mathbf{X}_{IJ}) \text{ and} \\ \boldsymbol{\varepsilon}_{(NIJ) \times 1} &= (\boldsymbol{\varepsilon}_{11}, \boldsymbol{\varepsilon}_{21}, \dots, \boldsymbol{\varepsilon}_{I1}, \boldsymbol{\varepsilon}_{12}, \dots, \boldsymbol{\varepsilon}_{IJ})^T.\end{aligned}$$

Let $\Sigma \in \mathbb{R}^{NIJ \times NIJ}$ be a sparse block diagonal covariance matrix composed of the matrices $\Sigma_1, \dots, \Sigma_J$. Hence, the log-likelihood of the aggregated data model in Equation (9) can be written as

$$\ell(\Theta; \mathbf{y}) = -\frac{1}{2} \log |\Sigma| - \frac{1}{2} (\mathbf{X}\boldsymbol{\beta} - \mathbf{y})^\top \Sigma^{-1} (\mathbf{X}\boldsymbol{\beta} - \mathbf{y}). \quad (10)$$

Equation (10) configures a Gaussian process regression likelihood (Shi and Choi, 2011; Ramsay and Silverman, 2005). Let $\Theta_{\Sigma} = (\sigma, \omega, \beta^\eta)$ be the parameters describing the covariance matrix Σ . The estimator of β is obtained using weighted least squares and Θ_{Σ} is estimated using the *BFGS* Quasi-Newton numerical optimization method. The estimation steps are described as follows.

Fix a precision value $\xi > 0$. Given a sample \mathbf{y} , at run $r = 0$ get initial values for $\beta^{(0)}$. At run $r > 0$, do

1. Fix $\beta^{(r-1)}$ to obtain $\Theta_{\Sigma}^{(r)}$ by optimizing the log-likelihood in (10).
2. Fix $\Theta_{\Sigma}^{(r)}$ to obtain $\beta^{(r)}$ via

$$\beta^{(r)} = \left(\mathbf{X}^\top (\Sigma^{(r)})^{-1} \mathbf{X} \right)^{-1} \left(\mathbf{X}^\top (\Sigma^{(r)})^{-1} \mathbf{y} \right). \quad (11)$$

3. If

$$\left| \ell(\Theta^{(r)}; \mathbf{y}) - \ell(\Theta^{(r-1)}; \mathbf{y}) \right| < \xi,$$

then stop. If not, add one unit to run (r) and repeat.

The precision value $\xi > 0$, also called the convergence criterion, is typically set to 10^{-6} . Because the least squares estimator for β is unbiased and its expected value does not depend on Σ , the initial values for β can be obtained by fitting a linear model with no covariance structure for the aggregated data model.

To improve computational performance, (11) can be written in terms of the covariance matrices for each substation in the block diagonal matrix Σ , that is,

$$\beta^{(r)} = \left(\sum_{i=1}^I \sum_{j=1}^J \mathbf{x}_{ij}^\top (\Sigma_j^{(r)})^{-1} \mathbf{x}_{ij} \right)^{-1} \left(\sum_{i=1}^I \sum_{j=1}^J \mathbf{x}_{ij}^\top (\Sigma_j^{(r)})^{-1} \mathbf{y}_{ij} \right).$$

Conditions for identifiability. To ensure the existence of the inverse of the left-hand size of $\beta^{(r)}$ in (11) the number of substations in sample \mathbf{y} must be greater than the number of subject types. In other words, $J > C$. Also, to avoid multicollinearity, markets must be linearly independent, that is, there must be no $M \in \mathbb{R}$ such that $\mathbf{m}_j = M \mathbf{m}_{j'}$, for any $j \neq j'$.

3.5. Model-based clustering analysis

Assume that substations can belong to B distinct clusters depending on the similarity of their consumers typical curves. Let Z_j be the latent variable that identifies to which cluster substation j belongs, with π_b being the probability of substation j belonging to cluster b . In other words, for each substation $j = 1, \dots, J$, let Z_j be a random multinomial variable such that $\mathbb{P}(Z_j = b) = \pi_b$, for $b = 1, 2, \dots, B$ and $\sum_{b=1}^B \pi_b = 1$. It is assumed that given $Z_j = b$, the typical curve of a consumer of type c is given by $\alpha_{cb}(\cdot)$ and the aggregated load is a Gaussian process with mean function $\mu_{jb}(\cdot)$ and covariance function $\Sigma_{jb}(\cdot, \cdot)$, that is,

$$Y_{ij}(\cdot) | Z_j = b \sim GP(\mu_{jb}(\cdot), \Sigma_{jb}(\cdot, \cdot)),$$

where $\mu_{jb}(t) = \sum_{c=1}^C m_{jc} \alpha_{cb}(t)$ and therefore the introduction of the latent variable Z_j leads to a mixture of Gaussian process regression (Shi et al., 2005).

3.5.1. Clustering model likelihood and inference

Let \mathbf{y} be the vector of observed aggregated energy consumption over I days at J substations, as in Equation (8), let $\mathbf{z} = (z_1, \dots, z_J)$ be the vector of latent variables and $\boldsymbol{\pi} = (\pi_1, \dots, \pi_B)$ its associated parameters. Consider $\mathbf{y}_{\cdot j} = (\mathbf{y}_{1j}, \dots, \mathbf{y}_{Ij})^\top$, the observed data log-likelihood can be written as

$$\ell(\boldsymbol{\Theta}, \boldsymbol{\pi} | \mathbf{y}) = \sum_{j=1}^J \log \left(\sum_{b=1}^B \pi_b f(\mathbf{y}_{\cdot j} | z_j, \boldsymbol{\Theta}, \boldsymbol{\pi}) \right). \quad (12)$$

The direct maximization of Equation (12) to obtain parameter estimates is difficult due to the presence of the logarithm of a summation. Hence, we develop an Expectation-Maximization (EM) algorithm (Dempster et al., 1977; McLachlan and Krishnan, 2007), which performs an iterative maximization of Equation (12) using the joint distribution of \mathbf{y}_{ij} and \mathbf{z}_j , with the so-called complete data log-likelihood given by:

$$\begin{aligned} \ell(\boldsymbol{\Theta}, \boldsymbol{\pi} | \mathbf{y}, \mathbf{z}) &= \sum_{j=1}^J \sum_{b=1}^B \mathcal{I}(z_j = b) \left(\log f(\mathbf{y}_{\cdot j} | z_j; \boldsymbol{\Theta}) + \log \mathbb{P}(Z_j = z_j | \boldsymbol{\pi}) \right) \\ &= \sum_{j=1}^J \sum_{b=1}^B \mathcal{I}(z_j = b) \times \\ &\quad \left(\log \pi_b - \frac{1}{2} \sum_{i=1}^I [\log |\boldsymbol{\Sigma}_{jb}| + (\boldsymbol{\mu}_{jb} - \mathbf{y}_{ij})^\top \boldsymbol{\Sigma}_{jb}^{-1} (\boldsymbol{\mu}_{jb} - \mathbf{y}_{ij})] \right) + C, \end{aligned} \quad (13)$$

where, similarly to Equation (10), $\boldsymbol{\mu}_{jb}$ can be written as $\boldsymbol{\mu}_{jb} = \mathbf{X}_j \boldsymbol{\beta}_b$.

The E-step of the EM algorithm calculates the expected value of $\ell(\boldsymbol{\Theta}, \boldsymbol{\pi} | \mathbf{y}, \mathbf{z})$ in (13) with respect to the conditional distribution of \mathbf{Z} given the observed data and current parameter estimates $\boldsymbol{\Theta}^{(r)}$ and $\boldsymbol{\pi}^{(r)}$ at iteration r to obtain

$$\begin{aligned} Q(\boldsymbol{\Theta}, \boldsymbol{\pi} | \boldsymbol{\Theta}^{(r)}, \boldsymbol{\pi}^{(r)}) &\equiv \mathbb{E}_{\mathbf{Z} | \mathbf{y}, \boldsymbol{\Theta}^{(r)}, \boldsymbol{\pi}^{(r)}} [\ell(\boldsymbol{\Theta}, \boldsymbol{\pi} | \mathbf{y}, \mathbf{z})] \\ &= \sum_{j=1}^J \sum_{b=1}^B \mathbb{P}(Z_j = b | \mathbf{y}_{1j}, \dots, \mathbf{y}_{Ij}; \boldsymbol{\Theta}^{(r)}, \boldsymbol{\pi}^{(r)}) \times \\ &\quad \left(\log \pi_b - \frac{1}{2} \log |\boldsymbol{\Sigma}_{jb}| - \frac{1}{2} \sum_{i=1}^I (\boldsymbol{\mu}_{jb} - \mathbf{y}_{ij})^\top \boldsymbol{\Sigma}_{jb}^{-1} (\boldsymbol{\mu}_{jb} - \mathbf{y}_{ij}) \right) + C. \end{aligned} \quad (14)$$

The probability $\mathbb{P}(\cdot)$ in Equation (14) can be computed using Bayes Theorem and written as

$$\mathbb{P}(Z_j = b | \mathbf{y}_{\cdot j}; \boldsymbol{\Theta}^{(r)}, \boldsymbol{\pi}^{(r)}) = \frac{\left[\prod_{i=1}^I f(\mathbf{y}_{ij} | z_j = b; \boldsymbol{\Theta}_b^{(r)}) \right] \times \pi_b^{(r)}}{\sum_{b'=1}^B \left[\prod_{i=1}^I f(\mathbf{y}_{ij} | z_j = b'; \boldsymbol{\Theta}_{b'}^{(r)}) \right] \times \pi_{b'}^{(r)}},$$

where the product of densities is possible because independence among days $i = 1, 2, \dots, I$ is assumed.

In the M-step we maximize the function $Q(\cdot)$ in Equation (14) with respect to the parameters $\Theta = \{\beta, \Theta_\Sigma\}$ and π , where Θ_Σ contains the parameters β^η and ω of the covariance matrix Σ_{jb} described in Section 3.4. The E-step probabilities $\mathbb{P}(Z_j = b | \mathbf{y}_{\cdot j}; \Theta^{(r)}, \pi^{(r)})$ are treated as fixed in the M-step since they depend only on the previous parameter estimates. Let

$$p_{jb}^{(r)} \equiv \mathbb{P}(Z_j = b | \mathbf{y}_{\cdot j}; \Theta^{(r)}, \pi^{(r)})$$

and let $Q(\cdot)$ be written as a sum of two terms: one that depends only on π and another term that depends only on Θ , that is,

$$Q(\Theta, \pi | \Theta^{(r)}, \pi^{(r)}) = Q_1(\pi | \Theta^{(r)}, \pi^{(r)}) + Q_2(\Theta | \Theta^{(r)}, \pi^{(r)})$$

where

$$Q_1(\pi | \Theta^{(r)}, \pi^{(r)}) = \sum_{j=1}^J \sum_{b=1}^B p_{jb}^{(r)} \log \pi_b \text{ and} \quad (15)$$

$$Q_2(\Theta | \Theta^{(r)}, \pi^{(r)}) = -\frac{1}{2} \sum_{j=1}^J \sum_{b=1}^B p_{jb}^{(r)} (\log |\Sigma_{jb}| + \sum_{i=1}^I (\mathbf{X}_j \beta_b - \mathbf{y}_{ij})^\top \Sigma_{jb}^{-1} (\mathbf{X}_j \beta_b - \mathbf{y}_{ij})). \quad (16)$$

Because Q_1 does not depend on Θ , $\pi_b^{(r+1)}$ can be obtained by maximizing Equation (15) with respect to π_b , subject to $\sum_{b=1}^B \pi_b = 1$. Therefore, using Lagrange multipliers it can be shown that

$$\pi_b^{(r+1)} = \frac{1}{J} \sum_{j=1}^J p_{jb}^{(r)}, \quad (17)$$

for $b = 1, \dots, B$.

To obtain $\beta_b^{(r+1)}$ and $\Theta_\Sigma^{(r+1)}$, we use the so-called Expectation/Conditional Maximization (ECM) algorithm (Meng and Rubin, 1993; McLachlan and Krishnan, 2007), where Θ_Σ is set equal to $\Theta_\Sigma^{(r)}$ and Q_2 in (16) is maximized with respect to β_b to obtain

$$\beta_b^{(r+1)} = \left(I \sum_{j=1}^J \mathbf{X}_j^\top (\Sigma_{jb}^*)^{-1} \mathbf{X}_j \right)^{-1} \left(\sum_{i=1}^I \sum_{j=1}^J \mathbf{X}_j^\top (\Sigma_{jb}^*)^{-1} \mathbf{y}_{ij} \right), \quad (18)$$

for $b = 1, \dots, B$ and $\Sigma_{jb}^* = p_{jb}^{(r)} \times \Sigma_{jb}^{-1}$.

Next, β_b is set to its updated value $\beta_b^{(r+1)}$ and Q_2 is maximized with respect to Θ_Σ through numerical optimization algorithms to obtain $\Theta_\Sigma^{(r+1)}$. E and M steps are then iterated until convergence is reached, that is, when $|\ell(\Theta^{(r)}, \pi^{(r)}; \mathbf{y}) - \ell(\Theta^{(r-1)}, \pi^{(r-1)}; \mathbf{y})| < \xi$ for $\xi > 0$.

3.5.2. Initial values and number of clusters

Obtaining initial values for all parameters might be a challenge if no previous information is available to guide the initialization. In this work, the following approach is proposed for clustering and parameter initialization.

The first step is to fix the number of clusters B and the number of trials G . For each trial $g \in G$, each substation is randomly assigned to a cluster, where the number of substations in each cluster must be greater than the number of customer types to preserve model identifiability. For each trial g , the clusters are split into datasets with their respective substations, and a simple aggregated data model is fitted to each one. Then the model with the smallest squared error among the G trials is selected to provide an initial β_b . The initial π is the proportion of substations in each cluster and the winning trial can also be used to provide initial covariance parameters.

The total number of clusters B is highly dependent on previous user information. As a first step, one might use the suggested approach of multiple fits with different numbers of clusters to select the configuration with the smallest squared error, which implies in high computing cost, or one might use an approximation of Bayes factors to select the best number of clusters B (Schwarz et al., 1978). The latter approach is detailed in Section 3.6 and is the approach used in this work.

It is also possible to assume that B is a random variable and obtain its estimated value through its posterior probability using approaches like the reversible jump algorithm (Green, 1995), but with intensive computation.

3.5.3. Identifiability condition

As in Section 3.4, there are necessary conditions for model fitting. Because there are at least B times the number of parameters, the procedure requires $J > CB$, that is, the number of substations must be greater than the number of estimated typical curves. Furthermore, substation markets must not be proportional to ensure full rank matrices in least squares computations.

3.6. Model check

This section will examine how to assess the uncertainty of the estimated mean curves and their covariance parameters. Inferences on the disaggregated mean curves can be performed by taking the closed form of the parameters in (11) and (18), because they are functions of the Gaussian process $Y_{ij}(\cdot)$ (Shi and Choi, 2011; Tresp, 2001). In fact, it can be said that

$$\hat{\beta} \sim \text{Normal}(\beta, \mathbf{A}\Sigma\mathbf{A}^\top), \quad (19)$$

with $\beta \in \mathbb{R}^{CK}$ as the true expansion parameters and $\mathbf{A} \in \mathbb{R}^{CK \times NIJ}$ defined as $\mathbf{A} = (\mathbf{X}^\top \Sigma^{-1} \mathbf{X})^{-1} \mathbf{X}^\top \Sigma^{-1}$.

Using the distribution of $\hat{\beta}$ given by (19), confidence intervals can be determined based on the standard errors in the diagonal of $\mathbf{A}\Sigma\mathbf{A}^\top$. On the other hand, the covariance parameters

Θ_{Σ} are obtained by numerical optimization using the Quasi-Newton methods available in the R language (Fletcher, 2013; R Core Team, 2019), and the parameter standard errors can be obtained from the observed Hessian matrix \mathbf{H} , that is,

$$SE(\Theta_{cov}) \equiv \sqrt{\text{diag}(\mathbf{H}^{-1})}.$$

The proposed covariance structures make the aggregated data models a family of nested models, where the uniformly homogeneous one is a particular case of the homogeneous model which is a particular case of the complete model. Two model fits can be compared using the likelihood ratio test. Let \mathcal{M}_1 and \mathcal{M}_2 be the two aggregated data models to be compared, with \mathcal{M}_1 nested in \mathcal{M}_2 . Denote by $\ell(\mathcal{M}_1)$ and $\ell(\mathcal{M}_2)$ the log-likelihood of models \mathcal{M}_1 and \mathcal{M}_2 , respectively. Then the likelihood ratio statistic L is defined by

$$L = -2(\ell(\mathcal{M}_2) - \ell(\mathcal{M}_1)), \quad (20)$$

where the test statistic is asymptotically χ^2 distributed with degrees of freedom equal to the difference in the number of parameters between models.

When comparing clustering models, if they have the same number of clusters but different covariance structures, then the same approach can be used to compare them. However, to compare models with distinct numbers of clusters, the *Bayesian information criterion* (BIC) comparison is recommended (Shi and Wang, 2008). Let $\ell(\Theta, \pi; \mathbf{y})$ be the observed data log-likelihood and let $\hat{\Theta}$ and $\hat{\pi}$ be the maximum likelihood estimates, then the BIC is given by

$$BIC = -2\ell(\hat{\Theta}, \hat{\pi}; \mathbf{y}) + H \log(IJN),$$

where H is the total number of parameters, I the total number of days, J the number of substations and N the number of observed point in time. Simulation studies for Gaussian process mixtures have shown that models with the smallest BIC tend to have the correct number of clusters (Shi and Wang, 2008).

Finally, if a model has a good fit to the observed data, the residual curves can be expected to oscillate randomly around the zero line.

4. Analysis of UK electrical substation data

In this section we apply the proposed clustering and full aggregated data models to the electrical load profiles from twelve energy substations in the United Kingdom presented in Section 2. In what follows, Section 4.1 presents the results of the simple aggregated model fit, followed by the full aggregated model in Section 4.2. Finally, Section 4.3 describes the clustering analysis results.

4.1. Simple homogeneous aggregated data model

The simple homogeneous aggregated data model described in Section 2.1 assumes the same homogeneous dispersion and decay parameters for all customer types. This might be a naive

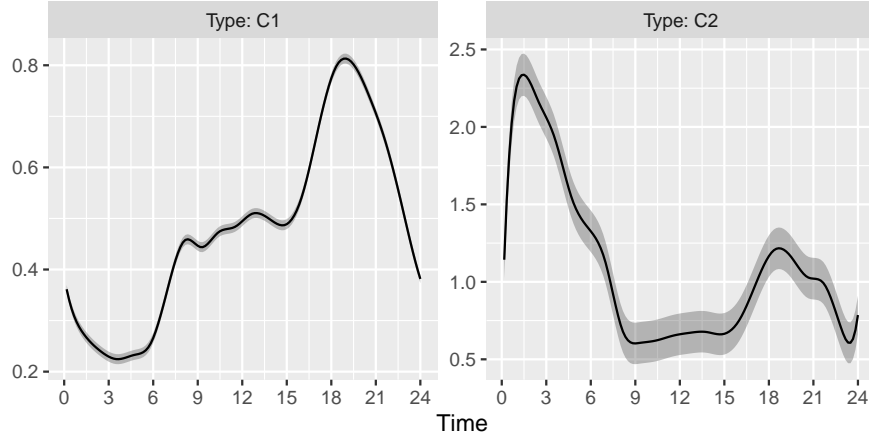


Fig. 3. Estimated typical curves in kWh and their confidence band (in gray) for unrestricted (C1) and “Economy 7” (C2) domestic customers using an homogeneous aggregated model.

approach, but its results can be used as initial values for the full model, drastically improving its computational performance.

Figure 3 displays the estimated typical curves considering 24 cubic B-Splines functions expansion. The unrestricted domestic (C1) customers consume less energy than “Economy 7” domestic (C2) customers. The typical consumption curve of C1 customers shows modest values early in the morning, rising to a higher baseline in the traditional work period between 9 AM and 4 PM to finally reach their peak at 7 PM and complete the cycle by slowly returning to low consumption late at night. On the right panel, the typical curve for C2 customers is almost a mirror image of C1: the curve has its peak right after midnight and is constantly decreasing until it reaches its lowest values at 9 AM, when the cheaper tariffs cease. Later, there is a local peak around 7 PM, higher than C1, but still considerably lower than the early morning peak.

Because both these customer types are domestic customers, certain behaviours can be conjectured to justify their typical curves. For example, unrestricted customers seem to have the habit of getting up in the morning and turning on electrical appliances that increase their load values, such as tea kettles, microwaves and hairdryers, for example. The work period presents many possibilities: most people leave their houses to go to work, decreasing home energy consumption, but some household members may stay at home to work in a home office. At night, when people arrive from their jobs, the appliances that are now turned on have higher energy consumption, such as washing machines and dryers that were not used in the morning. In contrast, the C2 typical curve has its major peak right after midnight, maybe due to appliances with higher energy cost making use of cheaper tariffs. From 9am onward both typical curves increase their loads up to a plateau until approximately 4pm, where the consumption rapidly increase to the local peak. Furthermore, the confidence band for the C2 typical curve is larger than for C1 because the C1 class contains most of the

Table 2. Estimated covariance parameters of the simple homogeneous aggregated data model for the UK electrical energy dataset.

Parameter	Type	Value	95% Confidence Interval
σ_c	C1	0.6608	(0.6452, 0.6764)
	C2	5.6094	(5.4494, 5.7693)
ω_c	C1	0.0404	(0.0384, 0.0425)
	C2	0.8205	(0.7721, 0.8689)

market share (around 90% or more) in most substations (see Table 1), and consequently the amount of information available to estimate the C1 typical curve is greater than for C2.

The estimated covariance parameters for the homogeneous aggregated data model are displayed in Table 2. The dispersion parameter for C2 is considerably greater than for C1, with larger confidence bands in Figure 3. The small decay parameter for C1 indicates that correlation between energy consumption at two distinct points in time decays faster for C1 than for C2. This means that, given the same time window, energy consumption in C2 has a stronger dependence on values in its time neighbourhood than C1. Furthermore, the confidence intervals for the covariance parameters reveal no evidence in favour of the homogeneous uniform model because the intervals for each customer type do not overlap.

To evaluate whether the model is suitable for the available data, the fitted aggregated curve is plotted along with the observed data in Figure 4a. Apparently, the homogeneous model can capture the main features of the data, but fails to fit the aggregated load in some substations such as S4 and S12: S4 has overestimated fitted curves, whereas S12 has underestimated curves. This suggests that it might be interesting to add other explanatory variables, or dummy variables indicating these two substations in the full model approach because there appears to be a vertical shift of the fitted curves. Other small discrepancies are visible in other substations, but in general they follow the main features of the observed data.

Figure 4b shows the relative residual curves defined in Section 3.6 for each substation with a reference line at zero and their median curve in green. Ideally, the median should almost coincide with the zero-reference line, but note that there are curves positioned above or below the zero reference. Specifically, substations S4 and S12 are clearly under- and overestimated respectively. Furthermore, the homogeneous dispersion hypothesis does not hold for these data because the dispersion of the residual curves varies over time, which is another piece of evidence in favour of the complete aggregated data model with variance functionals to capture this feature.

Important insights can be extracted from the homogeneous model fit before proceeding to the next level of the aggregated model, that is, the full model approach with additional covariates and a complete covariance structure. The bias in the fitted values for substations S4 and S12 suggests that indicator variables specific to these substations could be used as explanatory variables in the full model. In addition, the air temperature information is incorporated as a functional covariate to build the typical surface and potentially reduce the residual curves dispersion in the work period between 9am and 5pm.

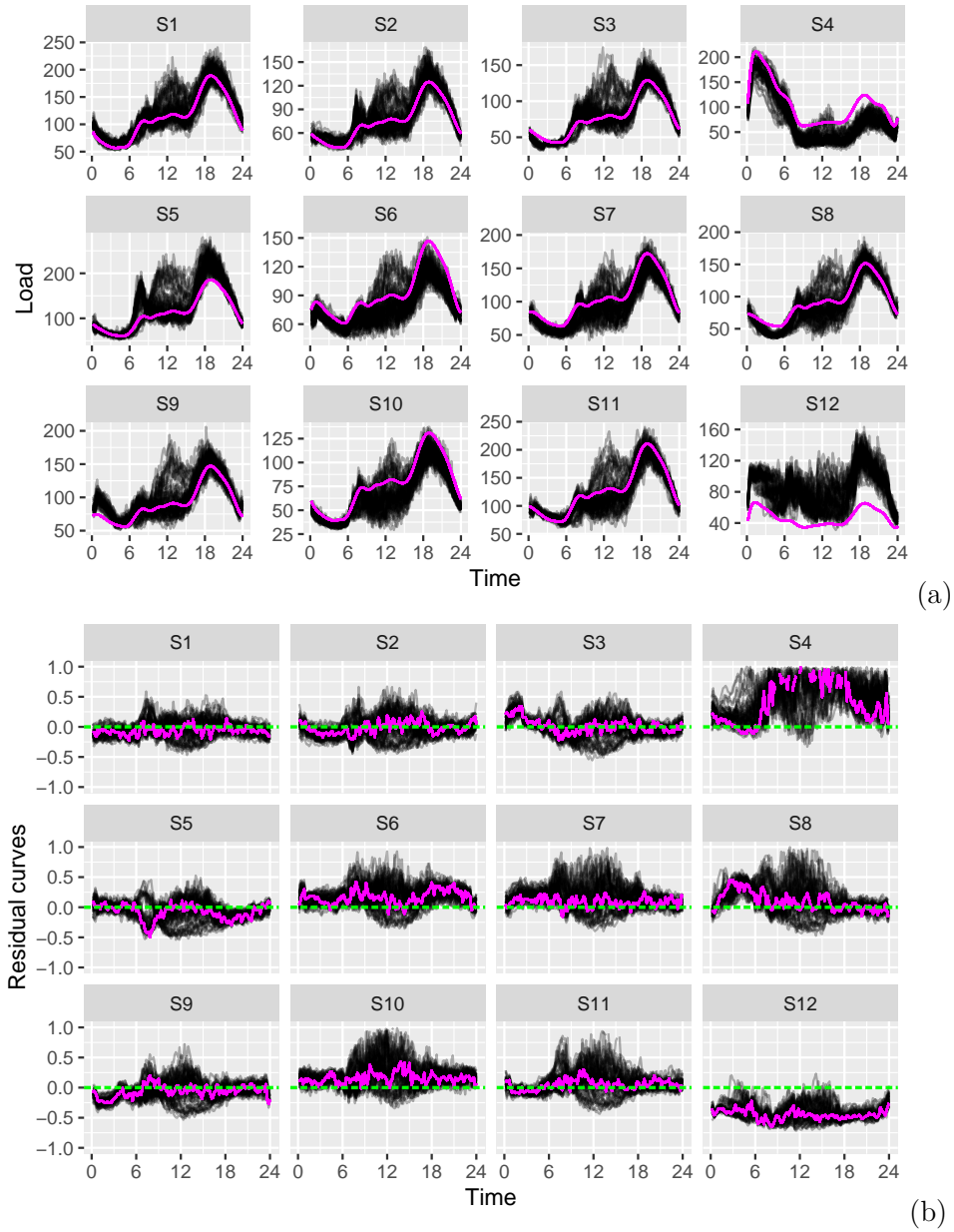


Fig. 4. Simple homogeneous aggregated data model fit: (a) observed aggregated curves in kWh (in gray) and fitted aggregated curves (in magenta) and (b) Relative residual curves (in gray), median residual curve (in magenta) and zero reference line (in green) for each substation.

Table 3. Summary statistics of air temperature in degrees Celsius over the 61 observed days in the dataset for each substation primary (Q = Quartile).

Primary	Minimum	1st Q	Median	3rd Q	Maximum
Cyncoed	-3.24	0.95	2.54	4.53	9.58
Llantarnam Primary	-4.22	0.89	3.30	7.90	12.06
Ringland Newport	-4.35	0.49	2.57	5.37	12.29
Trowbridge Primary	-5.41	-0.78	1.26	3.29	9.44
Usk	-6.27	1.00	5.74	8.07	12.22

4.2. Full aggregated data model

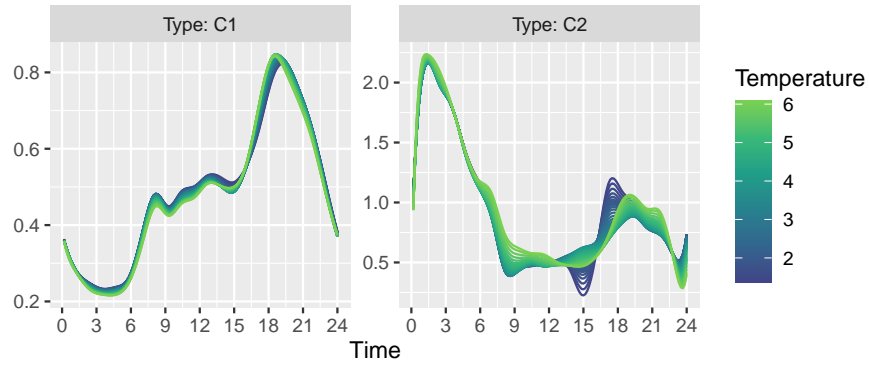
The full aggregated data model enables a functional covariate to be incorporated to produce typical surface responses for each customer type, as well as explanatory variables to better explain the aggregated data variability. For the tensorial product expansion in Equation (3), $K = 24$ and $L = 6$ are used to estimate the typical surface. In addition, two explanatory variables are considered as indicators of substations S4 and S12, as mentioned in Section 4.1. The variance functionals used in the complete covariance structure are expanded as in Equation (5) with $K' = 6$.

As mentioned in Section 2, temperature data were extracted for each primary every three hours, interpolated by cubic B-Splines and displayed in Figure 2b. Table 3 shows the summary statistics of the observed temperatures for each primary. Simulation studies (see Supplementary Material) showed satisfactory estimated typical surfaces for temperature intervals frequently observed in the data, but higher dispersion in the estimate for rarely observed temperatures. In the case of the UK data, except for Trowbridge, temperature data are concentrated approximately between 1°C and 4°C , and therefore the estimated typical surfaces may be well estimated within this range, but present some difficulties outside it.

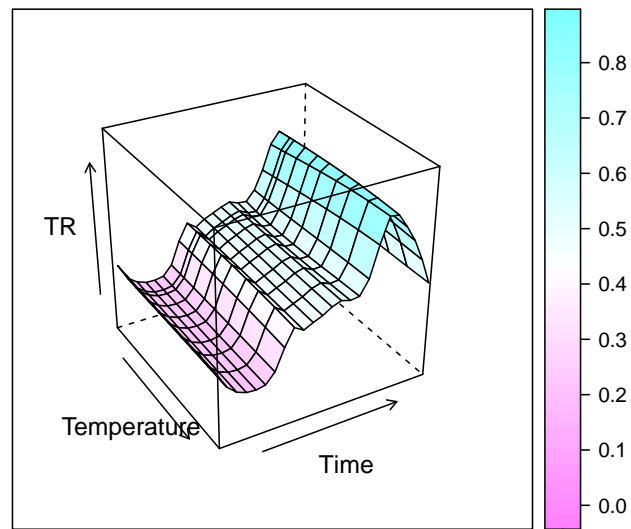
4.2.1. Full aggregated data model

Figure 5a shows the estimated typical curves for certain fixed temperature values, and Figures 5b and 5c show the estimated typical surfaces for C1 and C2 customer types, respectively, for temperatures between 1.21°C and 5.89°C . The selected temperature range contains 60% of the observed values in the dataset. Hence, that is the interval where the typical surfaces are well estimated avoiding discrepant values that do not contribute to the analysis as shown in Section 1.3 of our Supplementary Material. On the time axis, the estimated typical surfaces have similar characteristics to the curves estimated by the simple aggregated model shown in Figure 3. On the temperature axis, unrestricted domestic C1 customers present robust behaviour for different temperatures, but C2 customers are subject to greater variation of energy consumption between 12 PM and 8 PM at different temperatures. In the latter case, extreme temperatures must be considered with caution because for values outside the selected range, the typical curves are unstable and may present negative or extremely high values.

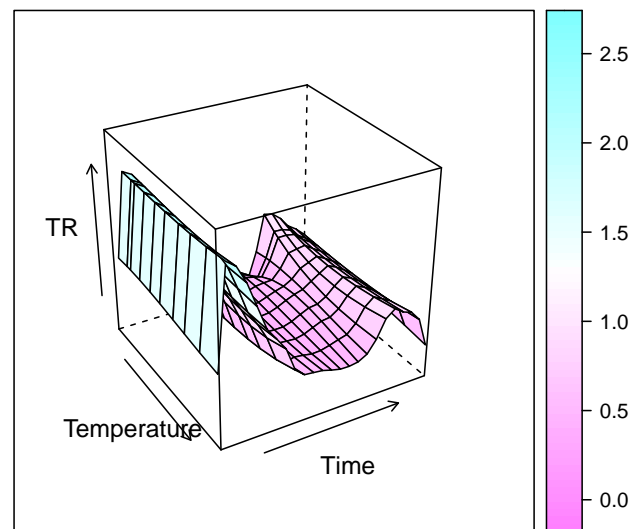
The first two lines of Table 4 show the estimated effect values for the dummy explanatory



(a)



(b)



(c)

Fig. 5. (a) Estimated typical curves in kWh for customers of type C1 and C2 coloured according to temperatures between 1.21°C and 5.89°, (b) estimated typical surface response in kWh for customers of type C1 between 1.21°C and 5.89°C and (c) estimated typical surface response in kWh for customers of type C2 between 1.21°C and 5.89°C. TR denotes the for typical response in kWh.

Table 4. Estimated coefficients of explanatory variables and estimated covariance parameters followed by their 95% confidence intervals using the full aggregated data model.

Parameter	Value	95% Confidence Interval
S12	37.3968	(33.5605, 41.2331)
S4	-8.1977	(-19.9304, 3.5350)
ω_{C1}	0.0333	(0.0313, 0.0353)
ω_{C2}	0.6127	(0.5803, 0.6450)

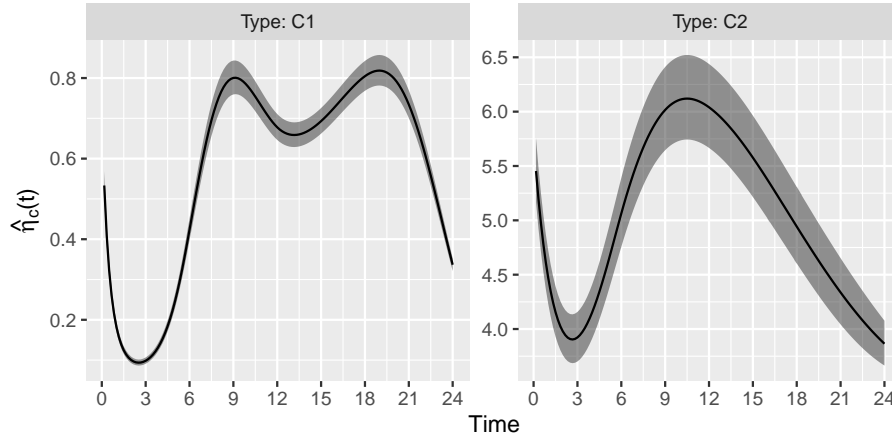


Fig. 6. Estimated variance functionals for C1 and C2 customers along with their confidence bands using the full aggregated data model.

variables corresponding to substations S4 and S12. Note that the estimated effect of substation S12 is a shift of 37.40, which is a considerable value because the aggregated observations in this location are mainly around 50 kWh and 120 kWh. Substation S4 results in an estimated effect of -8.20, but its 95% confidence interval contains zero, revealing that it may have no effect on the aggregated load data. The remaining lines of Table 4 present the estimated covariance decay parameters for C1 and C2 customers (ω_{C1} and ω_{C2}), which are much like to the ones obtained in Table 2. The correlation of neighbouring observations is stronger in type C2, with a decay parameter estimated at 0.61 versus 0.03 for type C1.

Figure 6 shows the estimated variance functionals for C1 and C2 customers along with their confidence bands built using their standard error as described in Section 3.6. The left panel reveals the higher values of dispersion at 9 AM, when people tend to leave their houses, and at 8 PM, the peak of the estimated typical curve. The lowest values are observed in early morning, a period with few or no activities in residences. On the right panel, note the peak around 10 AM and the lowest values around 10 PM and 3 AM. Interestingly, except for midnight, the lower tariff period has lower dispersion values.

Figure 7a shows the fit for the full aggregated data model along with the observed aggregated data. The over- and underestimation problem for substations S4 and S12 is solved by adding dummy variables, and including temperature captures a portion of data variability, but it is still difficult to explain the work period variability, which may be associated with other factors. Figure 7b presents the associated relative residual curves. Greater variability can be observed between 9 AM and 5 PM, but the residuals for S4 and S12 are closer to the zero-reference line than in Figure 4b.

4.2.2. Comparison with simple homogeneous aggregated data model

This section compares the proposed full aggregated data model with the simple homogeneous aggregated data model described in Section 4.1 to assess whether there are advantages to incorporating explanatory variables and temperature in terms of model fitting.

Table 5 shows the functional mean squared relative error (fMSRE) between fitted and observed values for each substation and fitted model given by:

$$\text{fMSRE}_j = \frac{1}{I} \sum_{i=1}^I \left\{ \frac{T}{N} \sum_{t=t_1}^{t_N} (\hat{y}_{ij}(t) - y_{ij}(t))^2 \right\}.$$

Except for substations S8 and S9, the full aggregated data model has smaller fMSRE for most substations. The larger differences are observed in S4 and S12, both substations that were not well fitted by the homogeneous aggregated model, as shown in Figure 4a. Considering all substations, the average fMSRE of the full model is better in terms of fMSRE, with a value of 0.208, whereas the homogeneous model has an average fMSRE of 0.266.

Because the homogeneous aggregated data model is nested inside the full aggregated data model, the likelihood ratio test can be performed to verify whether the model fits are statistically different. Hence, by designating the full model as \mathcal{M}_1 and the simple model as \mathcal{M}_2 , the test statistic L can be computed as

$$\begin{aligned} L &= -2(\ell(\mathcal{M}_1) - \ell(\mathcal{M}_2)) = -2(-344,770.3 - (-358,204.1)) \\ &= 26,867.67. \end{aligned}$$

Under the null hypothesis, the test statistic has approximately a chi-square distribution with 254 degrees of freedom obtained from the difference of the number of model parameters. Hence, the difference between the models is statistically significant with p -value very close to zero.

Therefore, the full aggregated data model is a better fit, improving the explanation of the aggregated load variability by adding the temperature component and dummy variables. The assumption of a complete covariance structure could capture the variability over time by means of the estimated variance functionals. Although the estimated surfaces might be used with caution in temperature ranges with few observations, in general they are useful to assess electrical energy consumption under different weather conditions. In addition, many other functional variables can be included in the model either as a higher-dimensional surface of additive linear or non-linear terms or as other explanatory variables, scalar or functional, to explain the aggregated data variability.

Table 5. Functional mean squared relative error (fMSRE) of fitted and observed data for each substation and fitted model.

Substation	Model	fMSRE
S1	Homogeneous	0.1350
	Full	0.1295
S2	Homogeneous	0.1527
	Full	0.1518
S3	Homogeneous	0.1636
	Full	0.1629
S4	Homogeneous	0.8097
	Full	0.3811
S5	Homogeneous	0.1713
	Full	0.1690
S6	Homogeneous	0.2390
	Full	0.2241
S7	Homogeneous	0.2279
	Full	0.2221
S8	Homogeneous	0.2485
	Full	0.2387
S9	Homogeneous	0.1609
	Full	0.1680
S10	Homogeneous	0.2763
	Full	0.2699
S11	Homogeneous	0.1733
	Full	0.1693
S12	Homogeneous	0.4389
	Full	0.2154

Table 6. Estimated probability \hat{p}_{jb} of substation j belonging to cluster b , under the two cluster fit.

	Trowbridge			Cyncoed		Ringland		Llantarnam				Usk
	S1	S2	S3	S4	S5	S6	S7	S8	S9	S10	S11	S12
\hat{p}_{j1}	1	1	1	1	0	1	1	1	1	1	1	0
\hat{p}_{j2}	0	0	0	0	1	0	0	0	0	0	0	1

4.3. Clustering analysis

The clustering aggregated data model groups substations with similar typical curves and covariance structure for domestic customers of type unrestricted and “Economy 7”. The model assumes that the aggregated observed data are a mixture of B aggregated models with distinct mean curves, with B as the total number of clusters. This section describes the fitting of a mixture of aggregated models with homogeneous covariance structure considering two and three clusters to obtain the best substation clustering that explains observed aggregated data variability using the Bayesian Information Criterion. There will be no explanatory variables or temperature components in this model. Models with four or more clusters do not meet the condition of identifiability to obtain typical curves and covariance parameter estimates because there are only 12 substations.

4.3.1. Two clusters

Figure 8 shows the estimated typical curves for customers of type C1 and C2 in Clusters 1 and 2. Type C1 curves share characteristics in both clusters like the increasing load around 9am, the plateau in the middle of the day, and the highest consumption at 8pm. Customers of type C2 have peaks at 2am in both clusters, but with different magnitudes, with Cluster 1 being the smaller one. The clustering aggregated model reveals new features for C2 customers, such as the different 8 PM peak, that could not be identified with the aggregated data models in Section 4.2.

Table 6 shows the estimated probability \hat{p}_{jb} of substation j being allocated to cluster b . Substations S5 and S12 are grouped in Cluster 2, and Cluster 1 gathers the remaining substations into a large cluster with 10 elements. Interestingly, S12 is the substation located far to the north, as shown in Figure 1, and one of the few substations that does not show an extreme dominance of C1 customer type; on the other hand, substation S5 has one of the markets dominated by C1 customers.

Figure 9a shows the fitted values plotted along with observed aggregated load data. Note that the model can explain most of the aggregated data variability. In contrast to the full homogeneous aggregated data model, the impact of the clustering approach is visible on substation S12. The fact that the model enables this substation to have an estimated typical curve different than most of the others shows that this clustering approach is sufficient to explain the electrical load variability without a dummy explanatory variable to shift estimated fitted values. In substation S5, this impact is not evident because C2 has only 3.11% of market share. Furthermore, the relative residual curves in Figure 9b shows that the clustering

Table 7. Estimated dispersion (σ_{cb}) and decay (ω_{cb}) parameters for customer type c in cluster b of the clustering aggregated model considering two clusters.

Parameter	Value	95% Confidence Interval
σ_{11}	0.7016	(0.6856, 0.7175)
σ_{21}	4.3629	(4.2214, 4.5045)
ω_{11}	0.0491	(0.0466, 0.0515)
ω_{21}	1.0033	(0.9406, 1.0661)
σ_{12}	1.5410	(1.4834, 1.5985)
σ_{22}	1.5375	(1.461, 1.6139)
ω_{12}	0.1588	(0.146, 0.1716)
ω_{22}	0.0277	(0.0244, 0.0310)

aggregated model has median residual curve oscillating around the zero reference line and indicating that it is well adjusted to the observed data. However, the difference in variability over time in the residual curves suggests that the complete covariance structure with variance functionals might be more suitable.

The estimated covariance parameters for both clusters are displayed in Table 7. When compared to the homogeneous model of Section 4.1, the estimated parameters of Cluster 1 are closer to those presented in Table 2. Still in Cluster 1, the results present a large estimated dispersion parameter for C2 customer types, possibly related to the small number of customers in the market and the difficulty of representing the variability of the period between 9 AM and 5 PM by a single typical curve.

In summary, the clustering aggregated data model with two clusters provides satisfactory fitted curves (see Figure 9) and typical curves that capture different characteristics for each cluster, especially customers of type C2. Even with no explanatory variables or additional temperature component it was possible to explain most of the variability of the load profiles.

4.3.2. Three clusters

The next step was to consider three clusters to fit the clustering aggregated data model assuming homogeneous covariance structure. Figure 10 shows the estimated typical curves for C1 and C2 for the three clusters. The unrestricted customers C1 have once more similar curves in all clusters, with small observable differences during the work period between 9 AM and 5 PM and at the 8 PM peak at night. In contrast, the “Economy 7” customers C2 have distinct estimated load profiles among clusters. The estimated C2 typical curve for Cluster 2 has the lowest energy consumption and its only peak in the early morning, whereas Clusters 1 and 3 share some characteristics like the double peak right after midnight and at 8 PM, but minor differences in the morning and during the work period.

The estimated cluster assignment probabilities are shown in Table 8, where each substation is allocated with high probability to its cluster. Again, S5 and S12 form one cluster whereas the the large cluster in Section 4.3.1 with 10 substations was divided into two clusters: one

Table 8. Estimated probability \hat{p}_{jb} of substation j belonging to cluster b , under the three cluster fit.

	Trowbridge			Cyncoed		Ringland		Llantarnam				Usk
	S1	S2	S3	S4	S5	S6	S7	S8	S9	S10	S11	S12
\hat{p}_{j1}	0	0	0	0	1	0	0	0	0	0	0	1
\hat{p}_{j2}	1	0	0	1	0	1	1	0	0	0	0	0
\hat{p}_{j3}	0	1	1	0	0	0	0	1	1	1	1	0

Table 9. Estimated dispersion (σ_{cb}) and decay (ω_{cb}) parameters for customer type c in cluster b of the aggregated three-cluster model.

Parameter	Value	95% Confidence Interval
σ_{11}	1.5367	(1.4798, 1.5936)
σ_{21}	1.5269	(1.495, 1.5588)
ω_{11}	0.1584	(0.091, 0.2258)
ω_{21}	0.0272	(-0.1216, 0.1761)
σ_{12}	1.0743	(1.0732, 1.0754)
σ_{22}	1.2794	(1.2762, 1.2825)
ω_{12}	0.1197	(0.1085, 0.1308)
ω_{22}	0.0905	(0.0159, 0.1650)
σ_{13}	0.4278	(0.4151, 0.4405)
σ_{23}	5.1783	(5.1706, 5.1859)
ω_{13}	0.0202	(0.0096, 0.0307)
ω_{23}	0.3743	(0.3487, 0.3998)

cluster composed by substations from Llantarnam primary and two from Trowbridge, and another cluster with Ringland substations plus S1 and S4. The clustering results show estimated typical curves that share some characteristics, but representing different morning and work period behaviors as seen in Figure 10.

The fitted curves over the observed aggregated data are displayed in Figure 11a. There are no apparent differences in fitted values compared to the two-cluster approach in Figure 9b. Recall that substation markets are mostly dominated by C1 customers, the ones with similar estimated typical curves in all clusters, with substations with more C2 customers like S4 and S12 remaining in the same cluster. Hence, the impact of different C2 typical curves for Llantarnam, for example, might not be evident in the estimated aggregated load. Therefore, the residual curves in Figure 11 yield the same characteristics as the two-cluster residual plot in Figure 9b. This figure suggests a good model fit represented by the median residual curves around the zero-reference line in most substations, except for a slight overestimation in substation S6. Comparisons between the two- and three-cluster models will be detailed in Section 4.3.3.

Table 9 displays the estimated covariance parameters for each combination of cluster and customer type. Cluster 1 probably has a homogeneous dispersion because the two values are

close, and their 95% confidence intervals overlap. However, there is high uncertainty in the decay parameters, especially for C2, where its confidence interval is large enough to contain zero, although we know this is not possible due to the parameter positive restriction. Cluster 2, the one with the lowest estimated C2 typical curves, has distinct dispersion and decay parameters for both customers and narrow confidence intervals. Lastly, Cluster 3 presents the largest distinction between dispersion parameters, which is visible in the confidence bands of the estimated typical curve of type C2 in Figure 10.

In summary, the clustering aggregated data model with three clusters divided the large cluster in the two-cluster approach into two groups represented mostly by their primaries. The estimated typical curves for customers of type C1 still show similarities between clusters, but now enable the estimated typical curves of C2 customers to accommodate three different electrical energy consumption profiles.

4.3.3. Model comparison

The two- and three-cluster aggregated data models resulted in good model fits according to the fitted values (Figures 9a and 11a) and the residual curves (Figures 9b and 11b). The difference between them can be observed in the large cluster with 10 substations for the two-cluster model, which is split into two clusters in the three-cluster model (Tables 6 and 8). To decide which model is best suited to the observed aggregated data, the model comparison tools described in Section 3.6 were used.

Table 10 shows the functional mean squared relative error (fMSRE) of the fitted and observed data under the two- and three-cluster models at each substation. In a comparison of substation fMSREs, S4 and S10 are highlighted because they have the largest differences between models. Observing both the fitted over observed values and the relative residual curves in Figures 9a and 9b under the two-cluster model, it is clear how far their median curves are from the zero-reference line. On the other hand, observing the same substations S4 and S10 in Figures 11a and 11b under the three-cluster model, it is apparent that their medians are closer to the zero line. In other words, the three-cluster model improves the model fit for these substations and consequently reduces their fMSRE. The other substations have minor differences between models in terms of fMSRE.

Another complementary tool is to compare the two models by their approximated BIC values. The two-cluster BIC is 707,308.3 and the three-cluster BIC is 704,571.4. Because the selection is favourable to models with the smallest BIC values, it again favours the aggregated three-cluster data model, although its BIC value is only 0.3% smaller than the BIC for the two-cluster model.

Therefore, the aggregated three-cluster model performed better in terms of fMSRE and BIC. Moreover, substations are grouped in a meaningful way, related to their primaries and avoiding the large cluster in the two-cluster approach. Hence, the three-cluster model seems to be a reasonable choice to group the electrical energy substations in the UK electrical load data.

Table 10. Functional mean squared relative error (fMSRE) of fitted and observed data under the two- and three-cluster models at each substation.

Substation	Clusters	fMSRE
S1	2	0.1330
	3	0.1403
S2	2	0.1552
	3	0.1569
S3	2	0.1676
	3	0.1663
S4	2	0.3009
	3	0.2354
S5	2	0.1603
	3	0.1603
S6	2	0.1818
	3	0.1678
S7	2	0.1971
	3	0.1851
S8	2	0.2284
	3	0.2636
S9	2	0.1750
	3	0.1584
S10	2	0.2689
	3	0.1739
S11	2	0.1590
	3	0.1633
S12	2	0.1977
	3	0.1977

5. Conclusion

The proposed aggregated data model has proved to be a useful tool to separate substation aggregated electrical load data into typical curves for each type of supplied customer and to comprehend their covariance structure. Our methodology includes novel approaches such as typical surface estimation as a function of time and temperature and explanatory variables and substation clustering based on the similarity of their estimated typical curves. By assuming a Gaussian process and using basis function expansions, our methodology becomes part of a family of functional models with favourable mathematical properties and well-established inference techniques.

Some estimation methods were crucial to the success of the proposed model, such as the least-squares estimator for the typical curves and the proposed initial value evaluation in the clustering approach in order to drastically reduce computing time and improve estimation performance.

The estimated typical curves demonstrated robustness to wrong covariance structure assumptions when analyzing the UK dataset in Section 4 as well as in simulated studies presented in the Supplementary Material. Furthermore, this work has assessed the results of misspecified scenarios and how they relate to the true parameters, for example, when scalar dispersion parameters are assumed instead of functional variances.

The full aggregated model with explanatory variables and additional functional component demonstrated sophistication and flexibility with both real and simulated data. Suggestions on how to use the additional component properly were provided to avoid poor decisions in temperature ranges with little information. In any case, when working with real data, the confidence intervals of the estimated typical curves and surfaces will indicate ranges of uncertainty.

Code availability

The methodology proposed in this work is implemented as an R package called `aggrmodel`, which is currently available online at the GitHub repository github.com/gabriel franco89/aggrmodel. The repository contains the functions used to perform all the analyses conducted in the paper as well as examples to illustrate package usability, which can be easily explored by the reader.

Supplementary Material

The file `supplementary_material.pdf` contains results from simulation studies conducted to show the performance of our proposed methods under various controlled scenarios.

Acknowledgements

This study was financed in part by the Coordenação de Aperfeiçoamento de Pessoal de Nível Superior – Brasil (CAPES) – Finance Code 001, by the National Science and Engineering

Research Council of Canada and FAPESP grant 019/00787-7. We thank Professor Gavin Shaddick for providing the data.

References

- Adjei, P., Sethi, N. S., de Souza, C. P. E. and Capretz, M. A. M. (2020) Energy disaggregation using multilabel binarization and gaussian naive bayes classifier. In *2020 11th IEEE Annual Ubiquitous Computing, Electronics Mobile Communication Conference (UEMCON)*, 0093–0100.
- Arghira, N., Hawarah, L., Ploix, S. and Jacomino, M. (2012) Prediction of appliances energy use in smart homes. *Energy*, **48**, 128–134.
- Basu, K., Debusschere, V., Bacha, S., Maulik, U. and Bondyopadhyay, S. (2014) Nonintrusive load monitoring: A temporal multilabel classification approach. *IEEE Transactions on industrial informatics*, **11**, 262–270.
- Bilski, P. and Winiecki, W. (2017) Generalized algorithm for the non-intrusive identification of electrical appliances in the household. In *2017 9th IEEE International Conference on Intelligent Data Acquisition and Advanced Computing Systems: Technology and Applications (IDAACS)*, vol. 2, 730–735. IEEE.
- Bouveyron, C., Bozzi, L., Jacques, J. and Jollois, F.-X. (2018) The functional latent block model for the co-clustering of electricity consumption curves. *Journal of the Royal Statistical Society: Series C (Applied Statistics)*, **67**, 897–915.
- De Souza, C. P., Heckman, N. E. and Xu, F. (2017) Switching nonparametric regression models for multi-curve data. *Canadian Journal of Statistics*, **45**, 442–460.
- Dempster, A. P., Laird, N. M. and Rubin, D. B. (1977) Maximum likelihood from incomplete data via the em algorithm. *Journal of the Royal Statistical Society: Series B (Methodological)*, **39**, 1–22.
- DeVore, R., Petrova, G. and Temlyakov, V. (2003) Best basis selection for approximation in l_p . *Foundations of Computational Mathematics*, **3**, 161–185.
- Dias, R. (1998) Density estimation via hybrid splines. *Journal of Statistical Computation and Simulation*, **60**, 277–293.
- Dias, R. and Garcia, N. L. (2007) Consistent estimator for basis selection based on a proxy of the kullback–leibler distance. *Journal of econometrics*, **141**, 167–178.
- Dias, R., Garcia, N. L., Ludwig, G. and Saraiva, M. A. (2015) Aggregated functional data model for near-infrared spectroscopy calibration and prediction. *Journal of Applied Statistics*, **42**, 127–143.

- Dias, R., Garcia, N. L. and Martarelli, A. (2009) Non-parametric estimation for aggregated functional data for electric load monitoring. *Environmetrics: The official journal of the International Environmetrics Society*, **20**, 111–130.
- Dias, R., Garcia, N. L. and Schmidt, A. M. (2013) A hierarchical model for aggregated functional data. *Technometrics*, **55**, 321–334.
- DUKES (2020) Digest of uk energy statistics (dukes). URL: https://assets.publishing.service.gov.uk/government/uploads/system/uploads/attachment_data/file/904805/DUKES_2020_Chapter_5.pdf.
- D’Oca, S., Corgnati, S. P. and Buso, T. (2014) Smart meters and energy savings in italy: Determining the effectiveness of persuasive communication in dwellings. *Energy Research & Social Science*, **3**, 131–142.
- Fletcher, R. (2013) *Practical methods of optimization*. John Wiley & Sons.
- Gouveia, J. P. and Seixas, J. (2016) Unraveling electricity consumption profiles in households through clusters: Combining smart meters and door-to-door surveys. *Energy and Buildings*, **116**, 666–676.
- Green, P. (1995) Reversible jump mcmc computation and bayesian model determination. *biometrika*, **82**: 711–732. hastings, wk 1970. monte carlo sampling methods using markov chains and their applications. *Biometrika*, **57**, 97–109.
- Hamidi, V., Li, F. and Robinson, F. (2009) Demand response in the uk’s domestic sector. *Electric Power Systems Research*, **79**, 1722–1726.
- Hart, G. W. (1992) Nonintrusive appliance load monitoring. *Proceedings of the IEEE*, **80**, 1870–1891.
- Hosseini, S. S., Agbossou, K., Kelouwani, S. and Cardenas, A. (2017) Non-intrusive load monitoring through home energy management systems: A comprehensive review. *Renewable and Sustainable Energy Reviews*, **79**, 1266–1274.
- Kim, Y., Kong, S., Ko, R. and Joo, S.-K. (2014) Electrical event identification technique for monitoring home appliance load using load signatures. In *2014 IEEE International Conference on Consumer Electronics (ICCE)*, 296–297. IEEE.
- Kohn, R., Marron, J. S. and Yau, P. (2000) Wavelet estimation using bayesian basis selection and basis averaging. *Statistica Sinica*, 109–128.
- Lenzi, A., de Souza, C. P. E., Dias, R., Garcia, N. L. and Heckman, N. E. (2017) Analysis of aggregated functional data from mixed populations with application to energy consumption. *Environmetrics*, **28**, e2414.
- Li, R., Gu, C., Li, F., Shaddick, G. and Dale, M. (2015a) Development of low voltage network templates—part i: Substation clustering and classification. *IEEE Transactions on Power Systems*, **30**, 3036–3044.

- (2015b) Development of low voltage network templates—part ii: Peak load estimation by clusterwise regression. *IEEE Transactions on Power Systems*, **30**, 3045–3052.
- Lin, Y.-H. and Tsai, M.-S. (2015) An advanced home energy management system facilitated by nonintrusive load monitoring with automated multiobjective power scheduling. *IEEE Transactions on Smart Grid*, **6**, 1839–1851.
- Luo, Z. and Wahba, G. (1997) Hybrid adaptive splines. *Journal of the American Statistical Association*, **92**, 107–116.
- McLachlan, G. and Krishnan, T. (2007) *The EM algorithm and extensions*, vol. 382. John Wiley & Sons.
- Meng, X.-L. and Rubin, D. B. (1993) Maximum likelihood estimation via the ecm algorithm: A general framework. *Biometrika*, **80**, 267–278.
- for National Statistics, O. (2016) 2011 census aggregate data. *Tech. rep.*, UK Data Service, DOI: <http://dx.doi.org/10.5257/census/aggregate-2011-1>.
- Prahastrono, I., King, D. and Ozveren, C. S. (2007) A review of electricity load profile classification methods. In *2007 42nd international universities power engineering conference*, 1187–1191. IEEE.
- R Core Team (2019) *R: A Language and Environment for Statistical Computing*. R Foundation for Statistical Computing, Vienna, Austria. URL: <https://www.R-project.org/>.
- Ramsay, J. and Silverman, B. (2005) *Functional Data Analysis*. Springer Science & Business Media.
- Schirmer, P. A. and Mporas, I. (2019) Integration of temporal contextual information for robust energy disaggregation. In *2019 IEEE 38th International Performance Computing and Communications Conference (IPCCC)*, 1–6. IEEE.
- Schirmer, P. A., Mporas, I. and Paraskevas, M. (2019) Evaluation of regression algorithms and features on the energy disaggregation task. In *2019 10th International Conference on Information, Intelligence, Systems and Applications (IISA)*, 1–4. IEEE.
- Schirmer, P. A., Mporas, I. and Sheikh-Akbari, A. (2020) Energy disaggregation using two-stage fusion of binary device detectors. *Energies*, **13**, 2148.
- Schwarz, G. et al. (1978) Estimating the dimension of a model. *The annals of statistics*, **6**, 461–464.
- Shi, H., Xu, M. and Li, R. (2017) Deep learning for household load forecasting—a novel pooling deep rnn. *IEEE Transactions on Smart Grid*, **9**, 5271–5280.
- Shi, J. and Wang, B. (2008) Curve prediction and clustering with mixtures of gaussian process functional regression models. *Statistics and Computing*, **18**, 267–283.

- Shi, J. Q. and Choi, T. (2011) *Gaussian process regression analysis for functional data*. Chapman and Hall/CRC.
- Shi, J. Q., Murray-Smith, R. and Titterton, D. (2005) Hierarchical gaussian process mixtures for regression. *Statistics and computing*, **15**, 31–41.
- Sousa, J. C., Jorge, H. M. and Neves, L. P. (2014) Short-term load forecasting based on support vector regression and load profiling. *International journal of energy research*, **38**, 350–362.
- Tresp, V. (2001) Mixtures of gaussian processes. In *Advances in neural information processing systems*, 654–660.
- Wang, Y., Chen, Q., Kang, C., Zhang, M., Wang, K. and Zhao, Y. (2015) Load profiling and its application to demand response: A review. *Tsinghua Science and Technology*, **20**, 117–129.
- Wilks, M. (2010) Demand side response: Conflict between supply and network driven optimisation. *A Report to DECC Nov*.
- Zhu, Y. and Lu, S. (2014) Load profile disaggregation by blind source separation: A wavelets-assisted independent component analysis approach. In *2014 IEEE PES General Meeting/Conference & Exposition*, 1–5. IEEE.

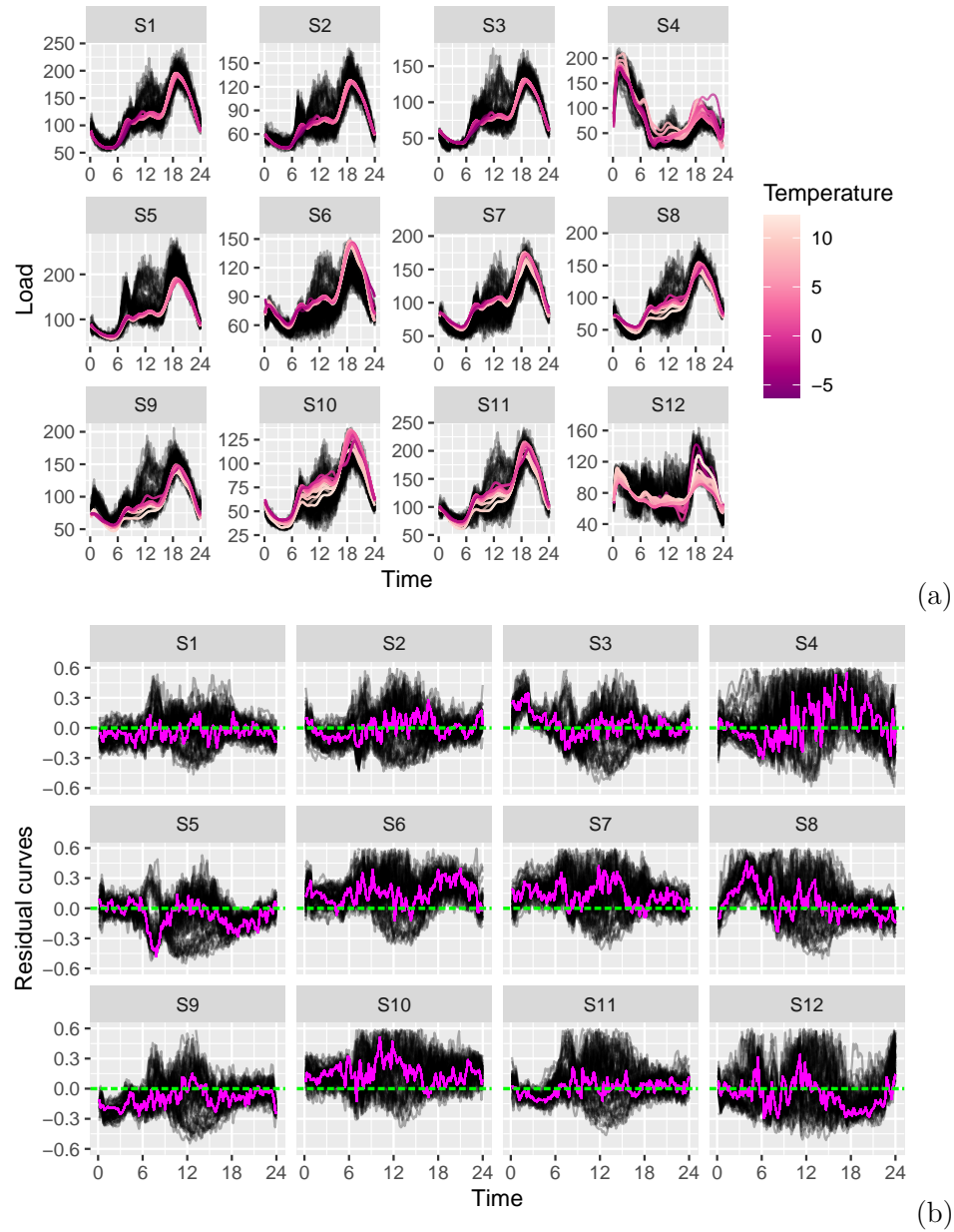


Fig. 7. Full aggregated data model typical curves results: (a) Observed aggregated load data (in gray) in kWh over estimated aggregated curves (in tones of magenta) and (b) relative error curves (in gray), median residual curves (in green) and zero reference line (in magenta) for the 12 substations using the full aggregated data model.

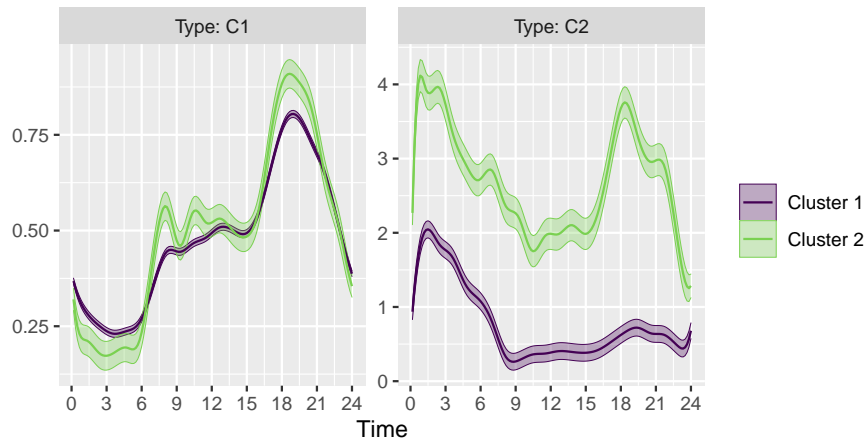


Fig. 8. Estimated typical curves in kWh and their confidence band for unrestricted (C1) and “Economy 7” (C2) domestic customers under two clusters aggregated data model fit.

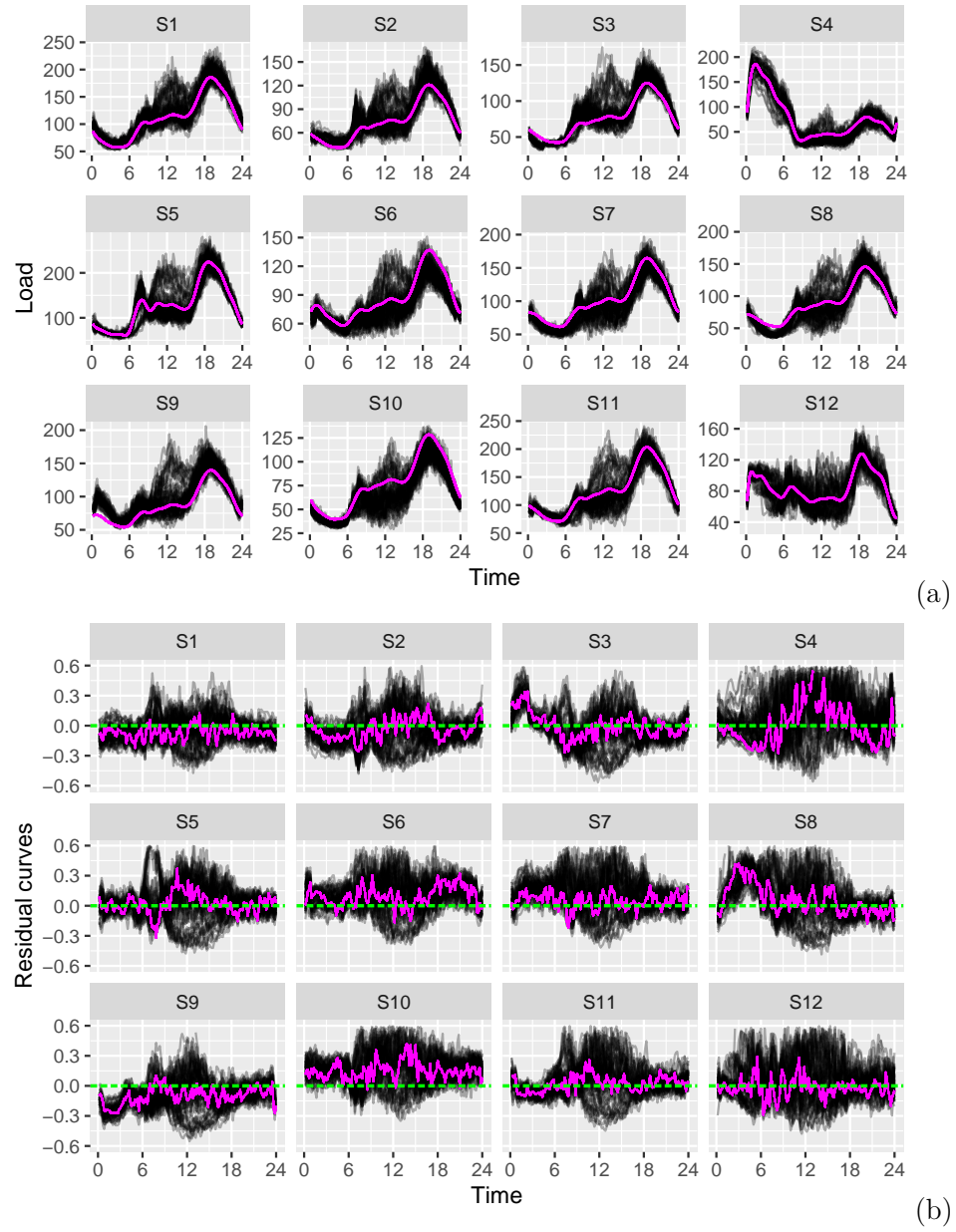


Fig. 9. Results of the clustering aggregated data model with two clusters: (a) Observed aggregated load data (in gray) in kWh over estimated aggregated curves (in magenta) and (b) relative error curves (in gray), median residual curves (in green) and zero reference line (in magenta) for the 12 substations.

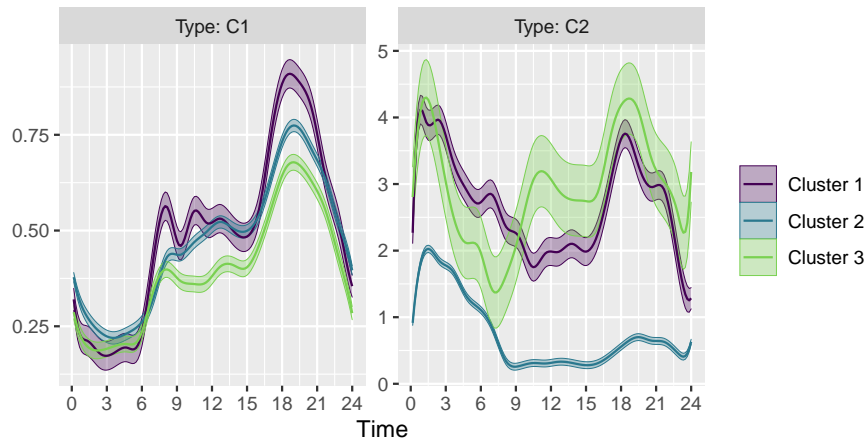


Fig. 10. Estimated typical curves in kWh and their confidence band for unrestricted (C1) and “Economy 7” (C2) domestic customers under three clusters aggregated data model fit

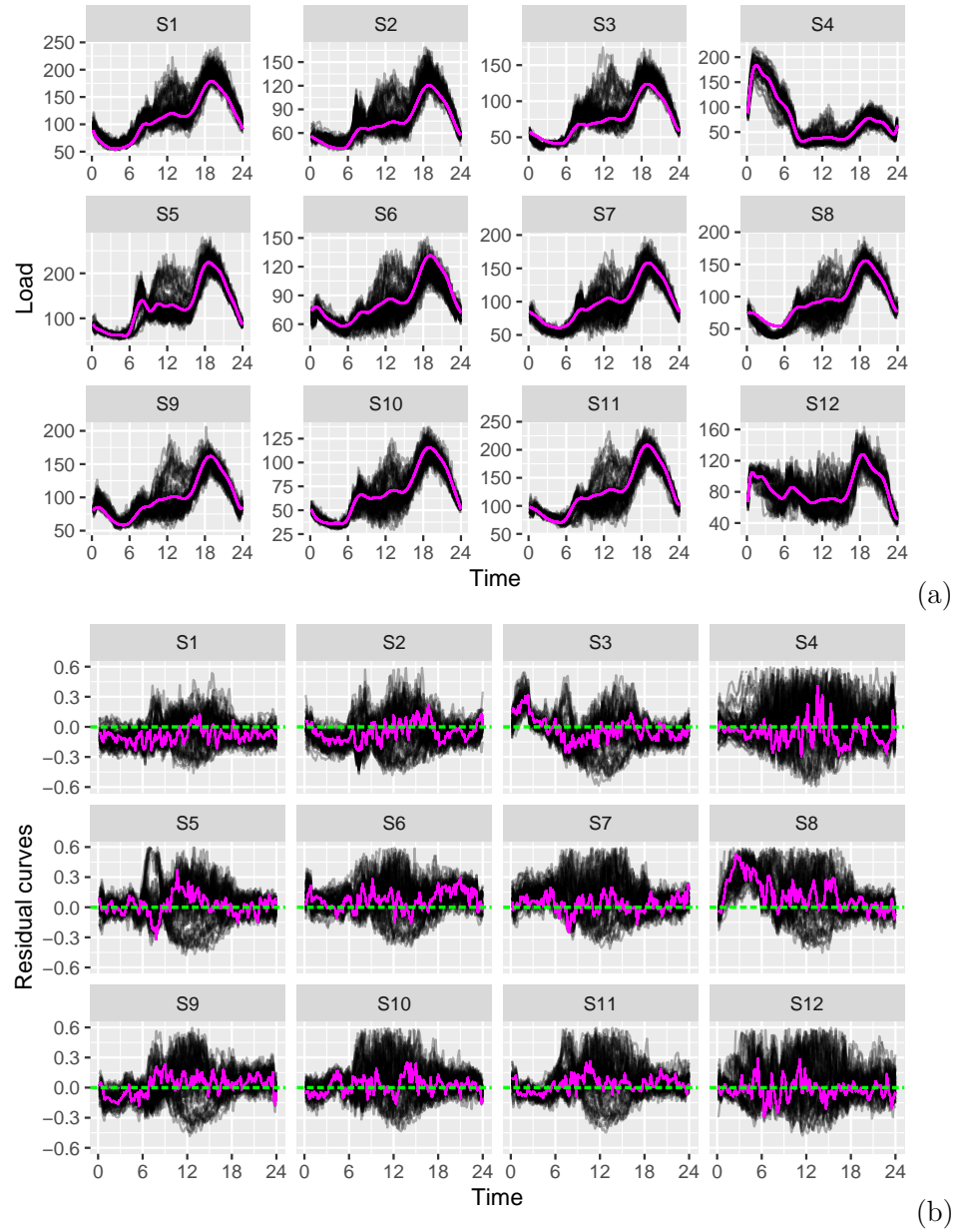


Fig. 11. Results of the clustering aggregated data model with three clusters: (a) Observed aggregated load data (in gray) in kWh over estimated aggregated curves (in magenta) and (b) relative error curves (in gray), median residual curves (in green) and zero reference line (in magenta) for the 12 substations.

Aggregated functional data model applied on clustering and disaggregation of UK electrical load profiles

Supplementary Material

Gabriel Franco, Camila P. E. de Souza and Nancy L. Garcia

Contents

1	Simulation studies	1
1.1	Simulation performance measures	2
1.2	Simulated scenario setup	2
1.3	Full aggregated data model	3
1.3.1	True parameters	3
1.3.2	Results	4
1.3.3	Discussion and conclusion	18
1.4	Clustering the aggregated model	18
1.4.1	Clustering setup and true parameters	20
1.4.2	Results	21
1.4.3	Discussion and conclusion	24
1.5	Additional tables	32

1 Simulation studies

This section evaluates the proposed aggregated data model in simulated scenarios. This approach provides control over the true model parameters that generate the data and the possibility of assessing the performance of estimated parameters in multiple simulation runs. All parameters used in our simulation studies are based on the estimated typical curves and estimated covariance parameters obtained from the analysis of the UK electrical energy substation data in Section 4 of the main paper.

Two independent simulation studies were performed: one for the full aggregated data model, and the other for the clustering aggregated data model. Section 1.1 describes the performance measures used to assess the quality of the estimated typical curves. Section 1.2 introduces the simulated scenarios for both studies. Section 1.3 presents the first study with its typical surface, explanatory variables and functional variance; focusing on the precision of the estimated parameters under two model fits: one considering a homogeneous covariance structure and the other a complete structure as in data generation. Section 1.4 describes the second study involving the clustering aggregated data model and its results. Section 1.5 contains two additional tables with results.

1.1 Simulation performance measures

To assess the performance of the estimated typical curves, the relative residual curve $R_c(t)$ of the customer of type c is defined as

$$R_c(t) = \frac{\hat{\alpha}_c(t) - \alpha_c(t)}{\alpha_c(t)}. \quad (1)$$

Analogously, the relative residual curve of the estimated variance functionals is also defined as

$$R_c(t) = \frac{\hat{\eta}_c(t) - \eta_c(t)}{\eta_c(t)}. \quad (2)$$

Division by the true value in (1) and (2) is desirable to make the residual curves comparable under different magnitudes.

Let R_{rc} be the relative residual curve of the customer of type c in the r -th simulation run. Define the functional Mean Squared Relative Error (fMSRE) as the mean of the integrals of the squared relative residual curves over time t . That is,

$$fMSRE_c = \frac{1}{R} \sum_{r=1}^R \int_0^T R_{rc}^2(t) dt \approx \frac{1}{R} \sum_{r=1}^R \left\{ \frac{T}{N} \sum_{t=t_1}^{t_N} R_{rc}^2(t) \right\}, \quad (3)$$

where N is the number of observed points in time in the data set and T the upper limit of the time domain. Because in this thesis the time frequencies are equally distanced, the fraction T/N is the equally spaced time difference band that approximates the dt of the integral on the left-hand side.

1.2 Simulated scenario setup

The simulated scenarios are different combinations of number of observed days, representing the amount of information available, and market balance, which is detailed below.

In real substation data, it is sometimes observed that a particular customer type may be overrepresented, with more than 95% of the market. If this dominance occurs in all observed substations, this situation is called an unbalanced market scenario, and a balanced market scenario otherwise. To study this phenomenon, the markets were generated as follows:

- Unbalanced: all substations have markets with more customers of Type 1 than Type 2 with percentage varying between 70% and 95%.
- Balanced: six substations have most of their customers of Type 1 and six substations have most of their customers of Type 2, with the majority percentages varying between 70% and 95%.

The percentages are relative to the number of customers for each substation, which is displayed in Table 1.

Table 1: Fixed number of customers for each substation in the simulation study.

Substation	1	2	3	4	5	6	7	8	9	10	11	12
Total	231	151	156	109	225	172	206	182	175	160	254	69

The combinations of market balance and number of observed days compose the eight different simulated scenarios presented in Table 2. Scenarios 1 to 4 are related to the full aggregated data model study and Scenarios 5 to 8 to the clustering aggregated data model study. Each scenario is composed of two types of customers observed at 30 minutes time frequency at 12 substations and replicated 15 times. In other words, 15 datasets were generated with these configurations and studied in detail, as described in Sections 1.3 and 1.4.

Table 2: Covariance structure, number of clusters, number of observed days, market balance and number of generated datasets (replicates). Eight simulated scenarios were proposed: Scenarios 1 to 4 for the full aggregated data models and Scenarios 5 to 8 for the clustering aggregated data model.

Scenario	Covariance	Clusters	Days	Market	Replications
1	Complete	1	5	Unbalanced	15
2	Complete	1	5	Balanced	15
3	Complete	1	30	Unbalanced	15
4	Complete	1	30	Balanced	15
5	Homogeneous	3	5	Unbalanced	15
6	Homogeneous	3	5	Balanced	15
7	Homogeneous	3	30	Unbalanced	15
8	Homogeneous	3	30	Balanced	15

1.3 Full aggregated data model

The full aggregated data model studies the typical surface together with explanatory variables related to substations. In this case, the surface is a function of time and daily air temperature, as presented in Section 3.2 of the main paper. Section 1.3.1 describes the air temperature functional and the explanatory variables used in this simulation, Section 1.3.2 presents the main results and Section 1.3.2 contains a discussion and the conclusions of this study.

1.3.1 True parameters

Recall the typical surface in Equation (3) introduced in Section 3.2 of the main manuscript:

$$\alpha_{ic}(t) = \alpha_{ic}(u(t), v_i(t)).$$

In this section, $u(t) = t$ and $v_i(t) = T_i(t)$ are used as the temperature at day i . Then, the typical surface is given by

$$\alpha_{ic}(t, T_i(t)) = b_c(t) \times \left(1 - \frac{1}{2}\Phi(T_i(t) - 1)\right), \quad (4)$$

with $b_c(t)$ as the baseline curve for customer of type c and $\Phi(\cdot)$ as the cumulative density function of the standard normal distribution. Hence when the temperature drops below 1°C the typical surface area increases considerably.

Figure 1 shows the baseline curves, the variance functionals and the signal-to-noise ratio (SNR) for each customer type. The SNR is simply the ratio of the typical curve to the variance functional at time t . The baseline curves and variance functionals were based on the estimated typical curves

obtained from the real data analysis in Section 4 of the main text. The type 1 baseline curve mimics the unrestricted domestic customer with lower consumption in early morning, increasing after 8 AM and reaching its peak at 8 PM. The Type 2 curve mimics the “Economy 7” customer with peaks around 2am and 8pm but with considerably larger electrical load values than Type 1. Customers variance functionals have higher values around the work period between 9am and 5pm, although Type 1 has two peaks that possibly represent when people leave from and arrive at their homes. The typical surfaces are shown in Figure 3.

The weather data containing temperature and air humidity were also based on real measurements for winter 2013 in Wales, United Kingdom. For this study, three sets of data were generated, representing three locations labelled T1, T2, and T3. Substations 1 to 4 were assigned to location T1, substations 5 to 8 to location T2, and the remaining substations 9 to 12 to location T3. Figure 2 shows the temperature and air humidity profiles for each location observed over 30 days. In fact, only data for scenarios 3, 4, 7, and 8 were generated in this manner. For scenarios 1, 2, 5, and 6, only the first five days were considered. In this study, temperature was used as the second component of the typical surface, and air humidity was used as an explanatory variable of the full aggregated data model with constant coefficient.

Furthermore, two explanatory variables were considered: air humidity as a functional variable, and a binary variable with value 1 for substations 1 and 2 and 0 otherwise, with associated coefficients $1/90 = 0.0111$ and 13, respectively. Therefore, from Section 3.2 of the main paper, the full aggregated complete model can be written as

$$Y_{ij}(t) = \left(\sum_{c=1}^C m_{jc} \alpha_c(t, T_i(t)) \right) + 13 D_{j1} + 0.0111 D_{ij2}(t) + \varepsilon_{ij}(t), \quad (5)$$

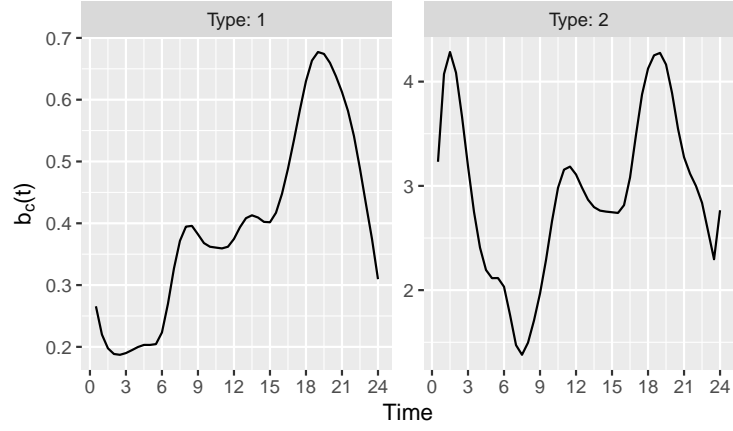
where D_{j1} is the dummy variable for substations 1 and 2 and $D_{j2} = D_{ij2}(t)$ the air humidity of substation j at time t of day i . Finally, the true covariance decay parameters for each customer type were defined as $\omega_1 = 0.03$ and $\omega_2 = 0.7$.

1.3.2 Results

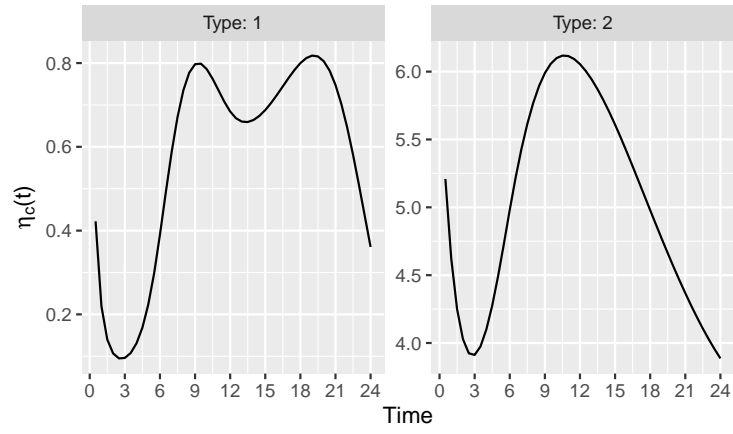
In this study, for each of Scenarios 1 to 4 in Table 2, two models were fitted: one homogeneous and one complete aggregated data model. The homogeneous fit tests the performance of typical surface estimation under an under-parameterized covariance structure and the behaviour of the dispersion parameters by reducing the variance functional to a scalar. On the other hand, the complete model tests check whether, under the correct scenario, the proposed model performs well in terms of typical surface and covariance parameter estimation.

Throughout this section, the number of observed days and the market balance are explicitly shown to avoid consulting Table 2 to remember the scenario setup.

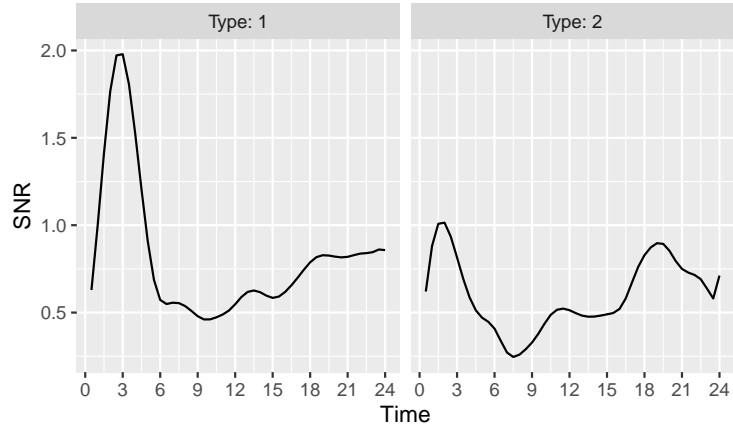
Starting with the homogeneous fit study, Figure 4 shows the estimated typical surfaces $\alpha_{ic}(t, T(t))$ for some temperature curves $T(t)$ for every combination of observed days and market balance. The first row in the panels represents a single instance of the temperature $T(t)$ on the first observed day in the simulated data and in its respective primary group T1, T2 or T3. Observe that Figures 4a and 4b show estimated typical surfaces with noticeable variability, where some curves assume negative values. However, the balanced scenario in Figure 4a presents estimated curves for Type 2 with lower variability than those in Figure 4b. On the lower panels, Figures 4c and 4d show lower variability than the five-day scenarios. Furthermore, observe that the estimated curves for Type 2 in Figure 4c have even lower variability. In general, the median curves in the four scenarios show that the



(a) Baseline curves



(b) Variance functionals



(c) Signal-to-noise ratio (SNR)

Figure 1: Baseline curves, true variance functionals and signal-to-noise ratio at time t of the simulation study.

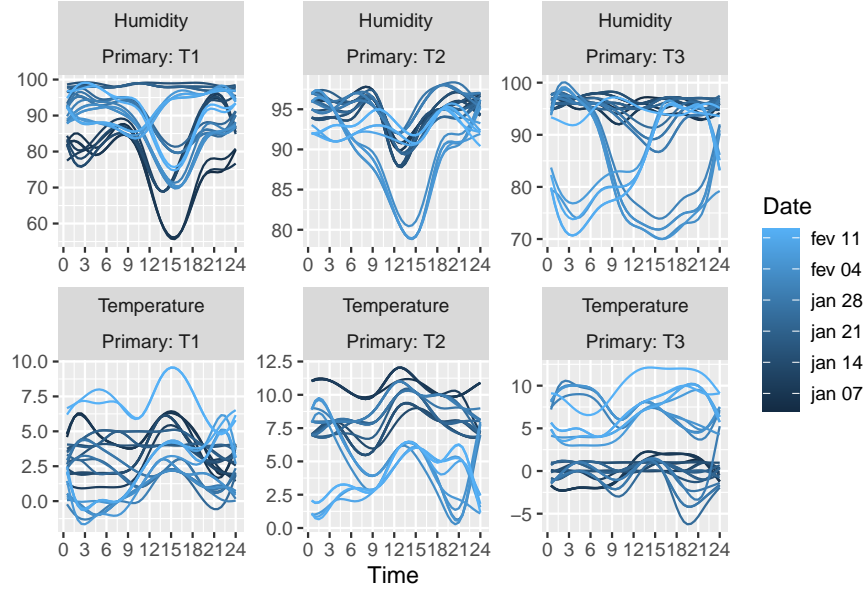
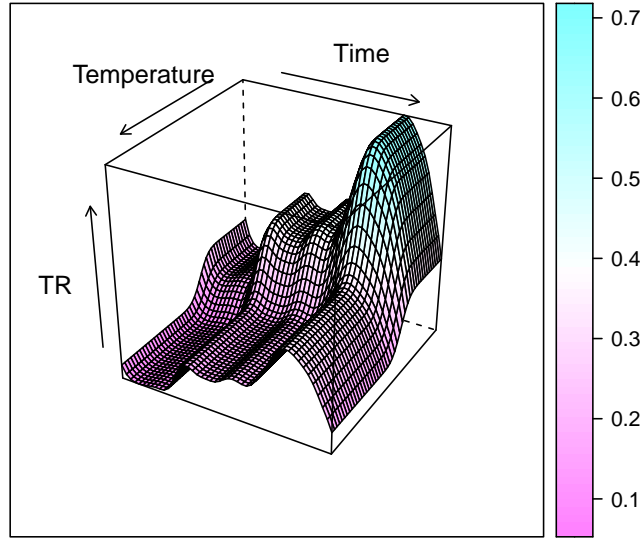


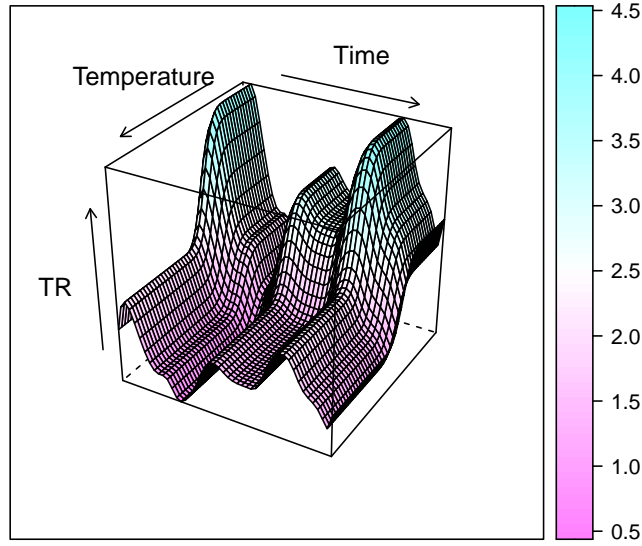
Figure 2: Air temperature and air humidity for each primary T1, T2 and T3 used in the simulation study.

estimated curves are concentrated around their true values. This proximity to the true curve is better visualized in the residual curves shown in Figure 5. As presented in Section 1.1, these curves are standardized so that the scenario performance can be compared. Note that the residual curves for Type 2 in the five-day scenarios have lower variability in Figure 5a than their respective ones in Figure 5b, as mentioned earlier. The same event occurs in the 30-day scenarios, but with lower variability than the five-day scenarios. The four panels of Figure 5 show median curves oscillating around the horizontal zero-reference line, with no major differences among scenarios. To summarize the precision of the estimated typical surfaces shown in Figure 4, Table 3 shows the functional Mean Squared Relative Error for Scenarios 1 to 4 fitted by the homogeneous model. Clearly, the fMSRE for the estimated Type 1 typical curves is considerably higher in the five-day scenarios. It seems that the magnitude of the curves influences the variability of the estimates because the curves with greater magnitude in Type 2 have lower fMSRE than those with lower magnitude in Type 1. Moreover, all fMSRE for the 30-day scenarios are lower than the respective ones in the five-day scenarios.

Figure 6a shows violin plots of the relative error of the estimated coefficients associated with the explanatory variables $\gamma_1 = 13$ and $\gamma_2 = 0.0011$. One run was excluded from the plot in the balanced scenario because it showed an absolute relative error greater than 38. In all scenarios, the estimates with γ_2 have larger violins than those with γ_1 . The 30-day scenarios have lower expected variability than the five-day scenario estimates, but their median reference lines above the zero line show visible underestimation of the parameter γ_2 . Furthermore, Table 4 shows the mean, median and square root of the Mean Squared Relative Error (srMSRE) of the estimated parameters. Observe that parameter γ_1 has estimates with considerably lower srMSRE than γ_2 .



(a) Typical surface for Type 1



(b) Typical surface for Type 2

Figure 3: Typical surfaces (TR) for each customer type as functions of time and the full range of observed temperatures in the three primaries.

The underestimation is notable in the mean and median values of γ_2 . Nevertheless, the statistics of parameter γ_2 show slight overestimation of the mean and larger srMSREs in all scenarios, especially the balanced five-day scenario, the one that presented a run with relative error greater than 38.

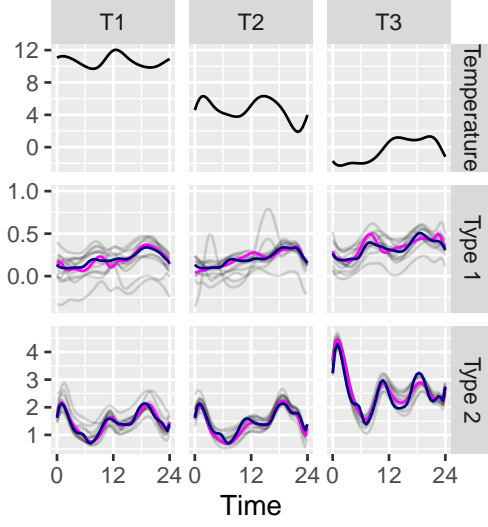
The estimated covariance parameters for Scenarios 1 to 4 are displayed in Figures 7 and 8 and Table 5. Figure 8 shows the estimated dispersion parameters represented over the true variance functionals, Figure 7 the violin plots of the estimated decay parameters and Table 5 the mean, median and square root of the Mean Squared Relative Error (MSRE) of the estimated decay parameters. Because the homogeneous model estimates a scalar as the dispersion parameter, the estimated values in Figure 8 are represented as constant lines over time. It seems that the horizontal lines are trying to capture an average of the variance functionals over time. In fact, taking the average of the variance functionals in Figure 8 over $t \in T$ yields 0.572 for Type 1 and 5.03 for Type 2, which are close to the respective median lines at 0.6324 and 4.6375. Moreover, the visibly overestimated value for Type 1 and the underestimated one for Type 2 in the unbalanced five-day scenario belong to the same run. On the other hand, the estimated decay parameters show systematic underestimation for Type 2 in all scenarios, as shown in Figure 7. The reduced estimate variability for the 30-day scenarios is observed only for estimated values of ω_2 . Again, the difference in magnitude of the parameters seems to have an influence on their performance, because $\omega_2 > \omega_1$. Furthermore, Table 5 shows the underestimation of ω_2 in the median and mean values and smaller srMSREs in favour of balanced markets in the five-day scenarios.

Figure 9 analogously shows the estimated typical surfaces for Scenarios 1 to 4 under the complete model fit. Again, observe that the estimated curve variability is reduced in the 30-day scenarios, especially for Type 2 under balanced markets. In addition, the advantage of balanced markets under the five-day scenarios can be seen from the lower variability of the residual curves in Figure 10 and the lower fMSRE in Table 3. The complete model does not present clear superiority in terms of fMSRE compared with the homogeneous model study.

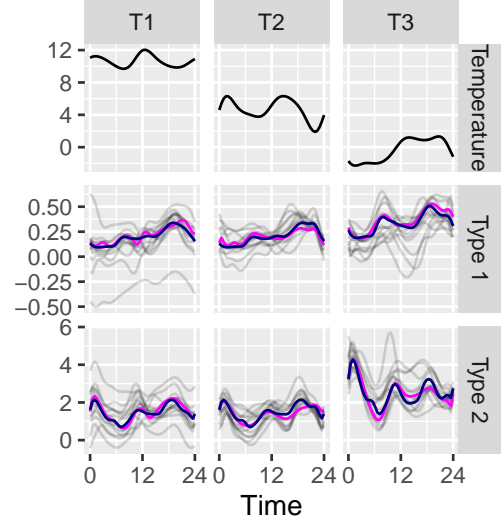
Figure 6b displays the relative errors of the estimated coefficients γ_1 and γ_2 associated with the explanatory variables. The characteristics of the violins are much like the respective ones in the homogeneous model. In fact, note that the srMSREs in Table 4 of both studies have similar values. Consequently, the complete model case shares the aspect of smaller srMSREs for estimates of γ_1 , especially in the 30-day scenarios.

Finally, Figure 11 shows the estimated variance functionals of the complete model and Figure 12 their respective residual curves. As observed in the typical curves, the 30-day scenarios present lower estimate variability than the five-day scenarios. In general, the estimates capture the main features of the true curves, such as the prolonged higher values for customers of Type 1 and the decreasing values after 12 AM for Type 2. However, in some regions, the estimated curves present behaviour different from the true curve. In all scenarios, observe that the Type 1 curves begin almost at zero, whereas the true curve has a small peak with rapid decay. Moreover, in the balanced 30-day scenario, the estimated variance functionals for Type 2 customers present a nonexistent local peak at the end of the day. The violin plots of the relative errors of the estimated decay parameters are displayed in Figure 13 and their summary statistics in Table 5. Essentially, the complete model offers estimates with smaller srMSRE compared with the homogeneous model, but the underestimation of ω_2 persists.

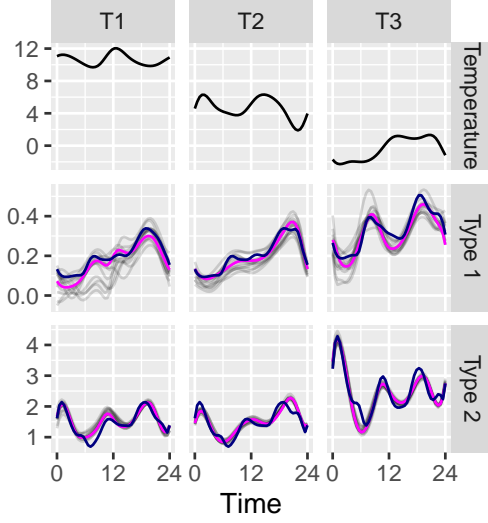
In addition, because the homogeneous model is nested in the complete model, Table 11 in Section 1.5 shows the likelihood ratio test for all runs in every scenario. In all cases the test favours the complete model fit with p-values smaller than 0.0001.



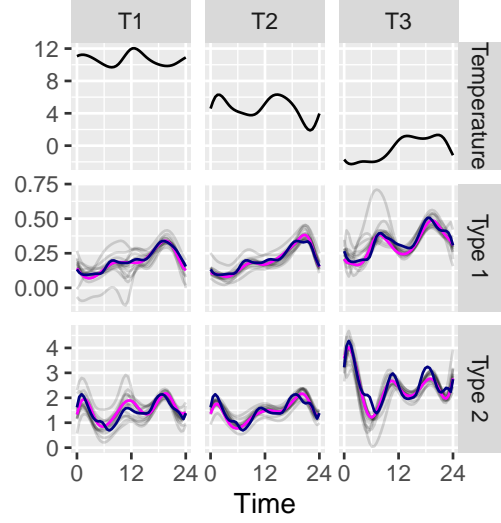
(a) Balanced market with 5-day data



(b) UnBalanced market with 5-day data



(c) Balanced market with 30-day data



(d) UnBalanced market with 30-day data

Figure 4: At every panel, the first row represents the temperatures $T(t)$ for each temperature set T1, T2 and T3; the following rows represent the estimated typical curves of $\alpha_c(t, T(t))$ for customers of Type 1 and 2 in Scenarios 1 to 4 under the homogeneous model fit. Median depth lines are represented in magenta, true typical curves in blue and estimated typical curves for each simulation run in gray.

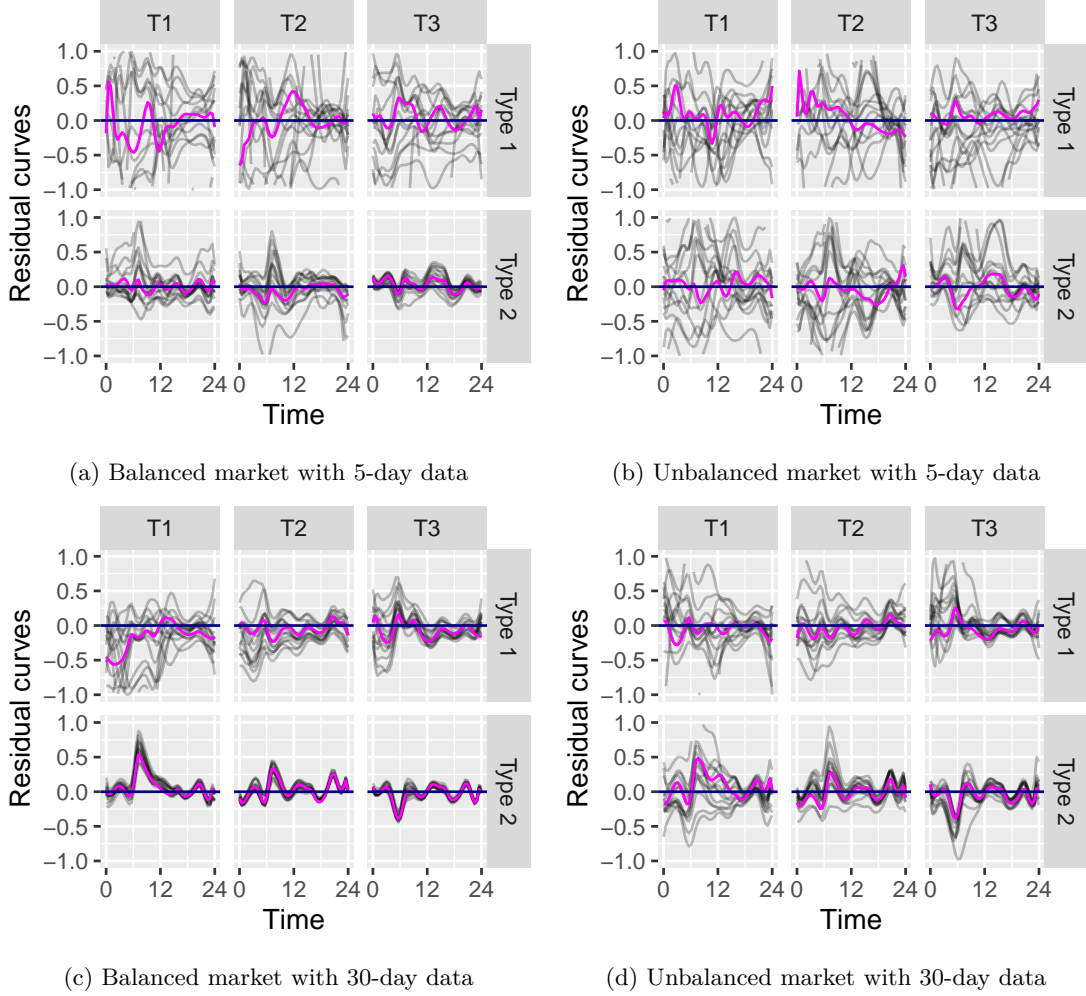
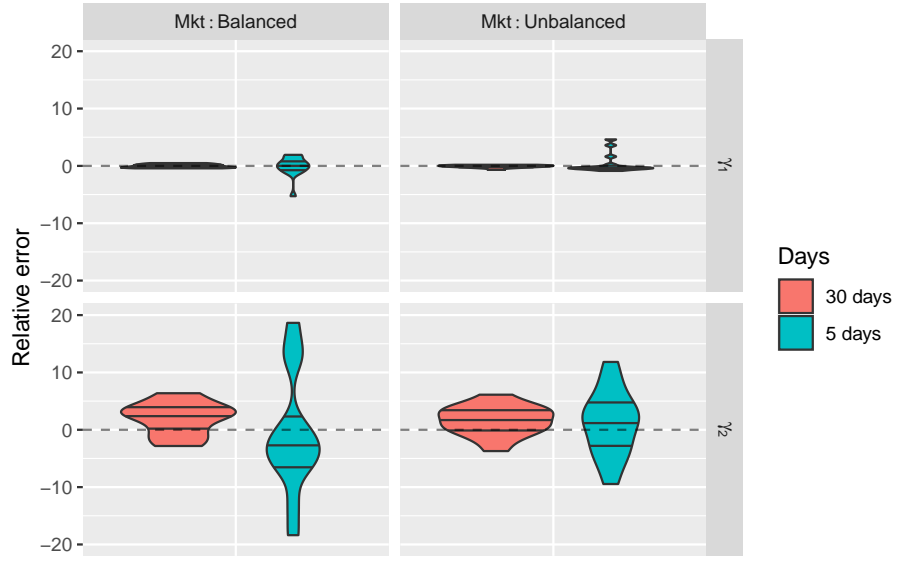


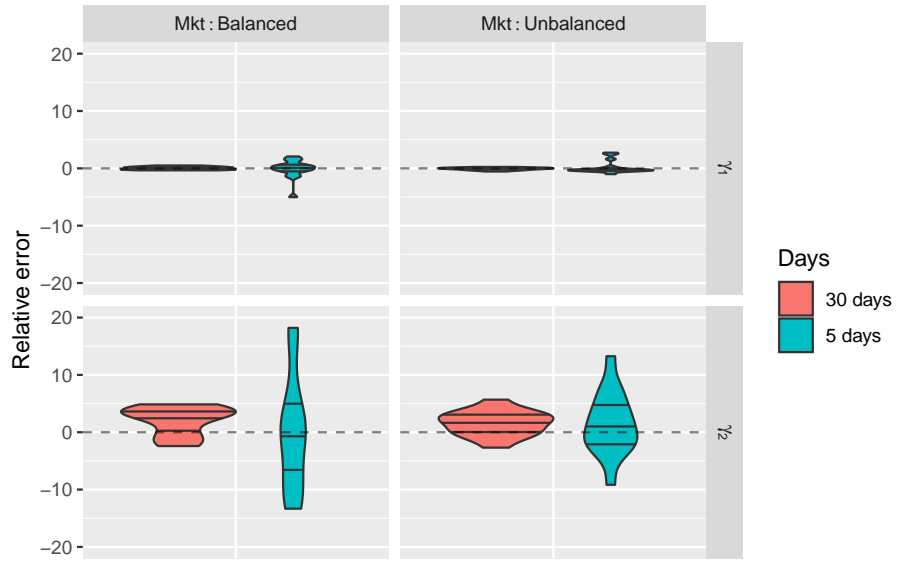
Figure 5: Residual curves of the estimated typical curves for Scenarios 1 to 4 in grey and their median depth in magenta under the homogeneous model fit in Figure 4.

Table 3: Functional mean squared relative errors of the estimated typical curves under the homogeneous (Figure 4) and complete (Figure 9) model fit for Scenarios 1 to 4.

Model	Days	Type	Market balance	fMSRE
Homogeneous	5 days	Type 1	Balanced	17.6706
			Unbalanced	18.4121
		Type 2	Balanced	0.8899
			Unbalanced	4.6557
	30 days	Type 1	Balanced	1.9525
			Unbalanced	2.1867
		Type 2	Balanced	0.5814
			Unbalanced	1.0923
Complete	5 days	Type 1	Balanced	19.5322
			Unbalanced	14.9073
		Type 2	Balanced	0.9747
			Unbalanced	3.9616
	30 days	Type 1	Balanced	1.9122
			Unbalanced	1.9651
		Type 2	Balanced	0.7720
			Unbalanced	1.1850

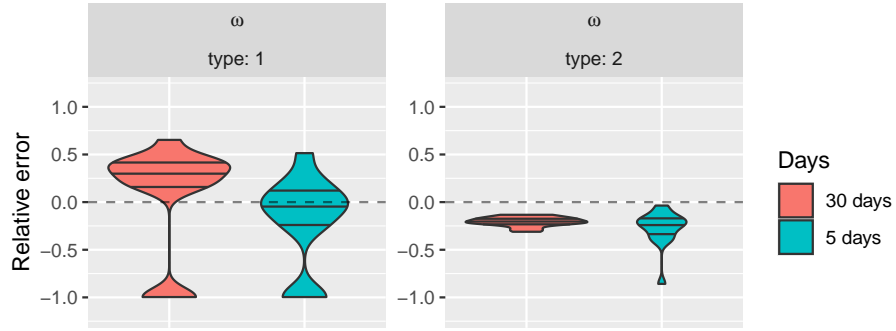


(a) Homogeneous covariance structure

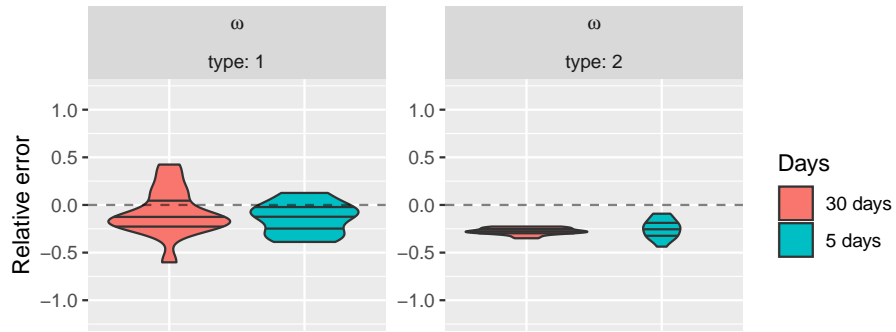


(b) Complete covariance structure

Figure 6: Relative errors of the estimated explanatory variables coefficients, $\gamma_1 = 13$ and $\gamma_2 = 0.0011$, and their relative error distribution under a) the homogeneous model fit and b) under the complete model fit for Scenarios 1 to 4.

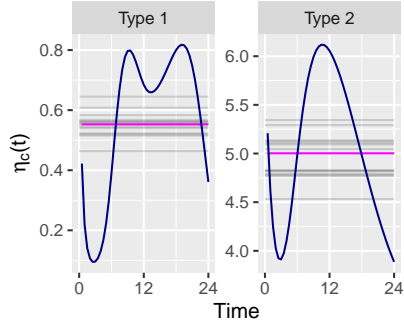


(a) Unbalanced market

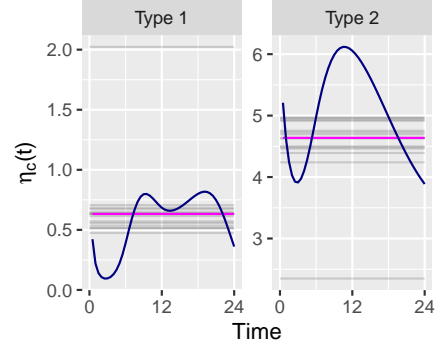


(b) Balanced market

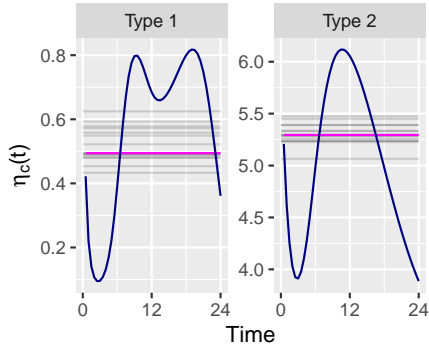
Figure 7: Relative errors of the estimated covariance parameters $\omega_1 = 0.03$ and $\omega_2 = 0.70$ under the homogeneous model fit for Scenarios 1 to 4.



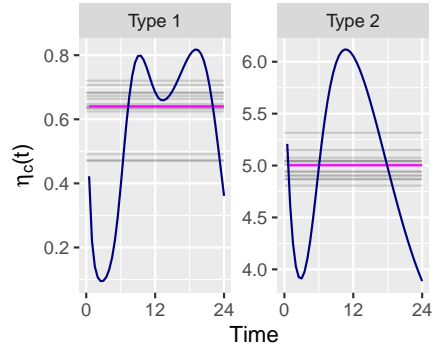
(a) Balanced market with 5-day data



(b) Unbalanced market with 5-day data

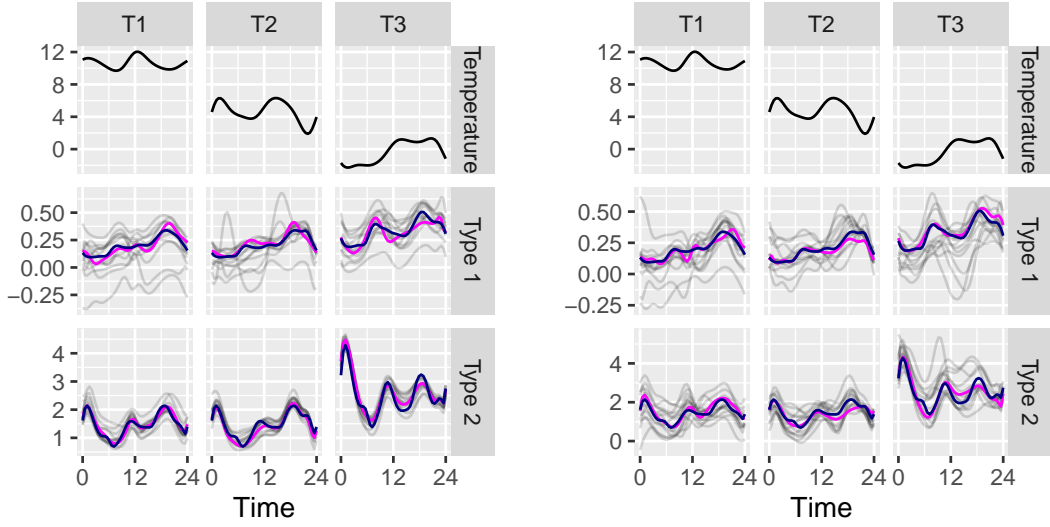


(c) Balanced market with 30-day data



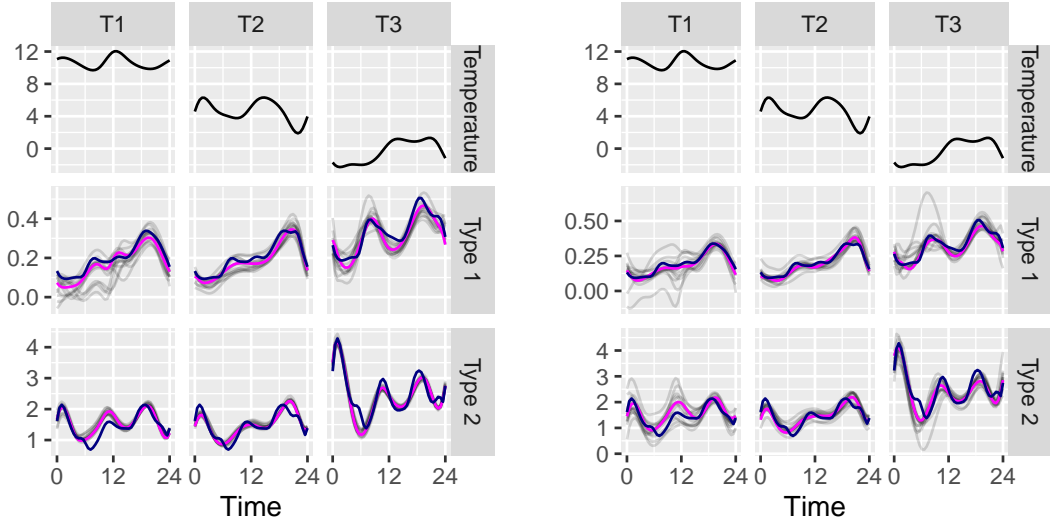
(d) Unbalanced market with 30-day data

Figure 8: Estimated dispersion parameters for Scenarios 1 to 4 under the homogeneous model fit represented by the horizontal gray lines. Median lines are represented in magenta and the true variance functionals in blue.



(a) Balanced market with 5-day data

(b) Unbalanced market with 5-day data



(c) Balanced market with 30-day data

(d) Unbalanced market with 30-day data

Figure 9: In every panel, the first row represents the temperatures $T(t)$ for each temperature set T1, T2 and T3; the following rows represent the estimated typical curves of $\alpha_c(t, T(t))$ for customers of Type 1 and 2 in Scenarios 1 to 4 under the complete model fit. Median depth lines are represented in magenta, true typical curves in blue and estimated typical curves for each simulation run in gray.

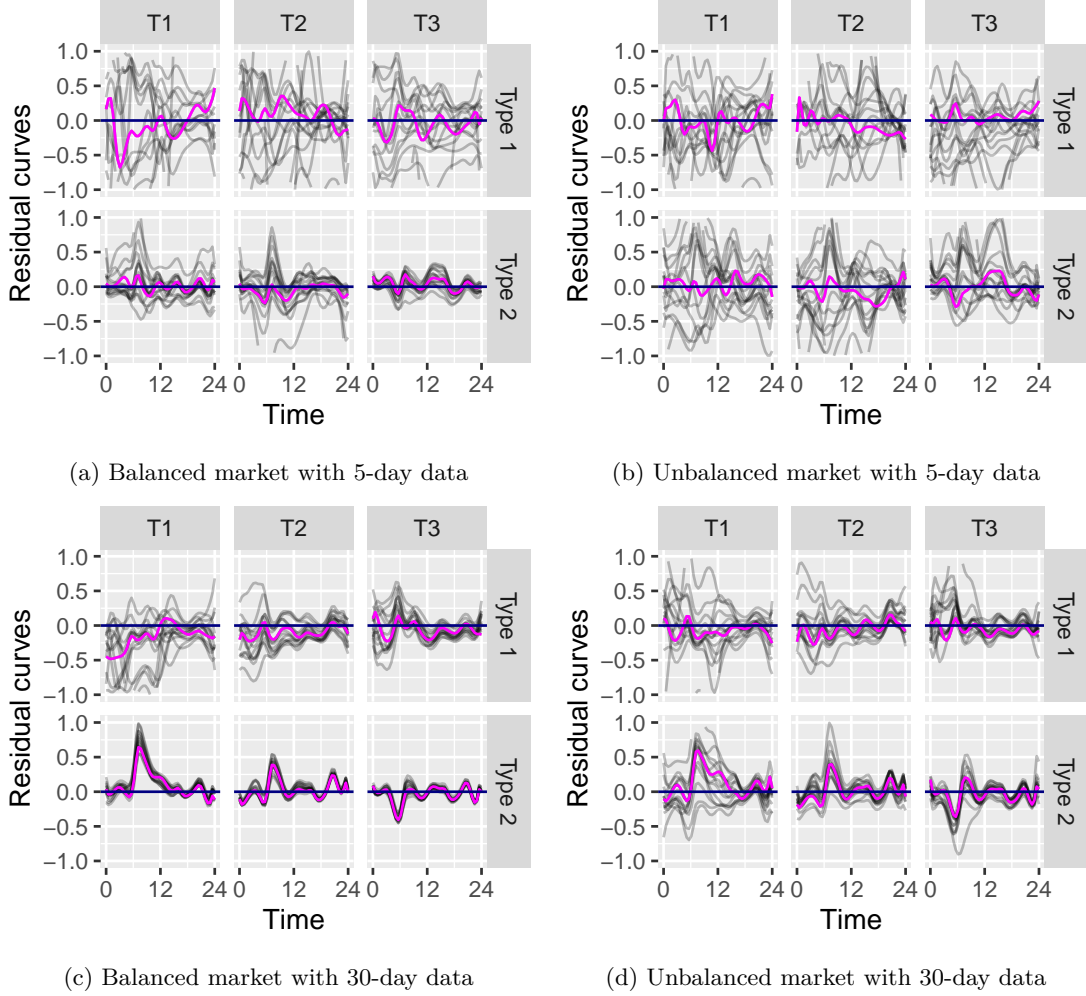
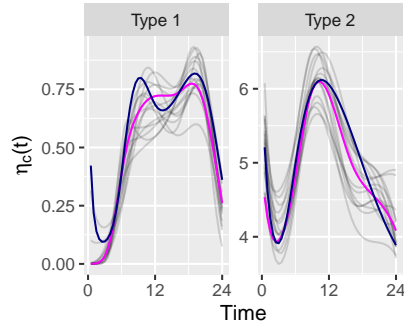
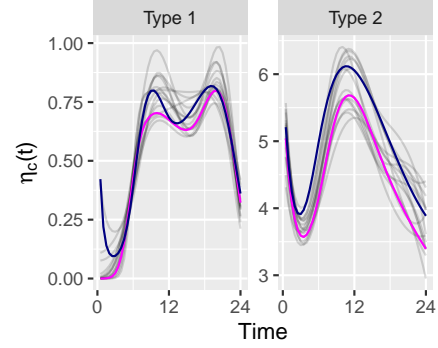


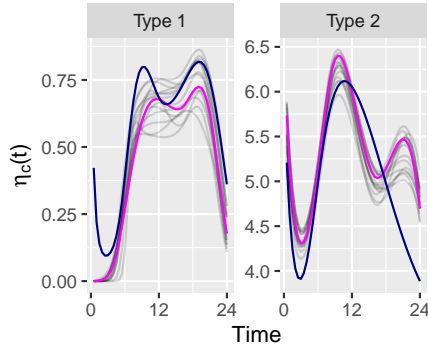
Figure 10: Residual curves of the estimated typical curves in grey and their median depth in magenta under the complete model fit in Figure 9.



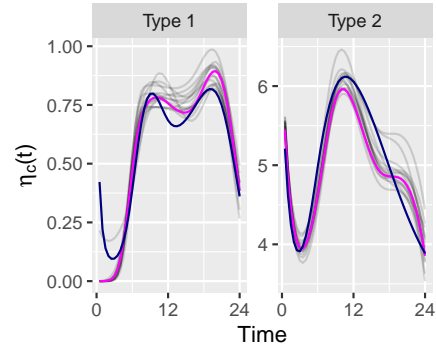
(a) Balanced market with 5-day data



(b) Unbalanced market with 5-day data



(c) Balanced market with 30-day data



(d) Unbalanced market with 30-day data

Figure 11: Estimated variance functionals for Scenarios 1 to 4 under the complete model fit. Median depth lines are represented in magenta, true variance functionals in blue and estimated curves in gray.

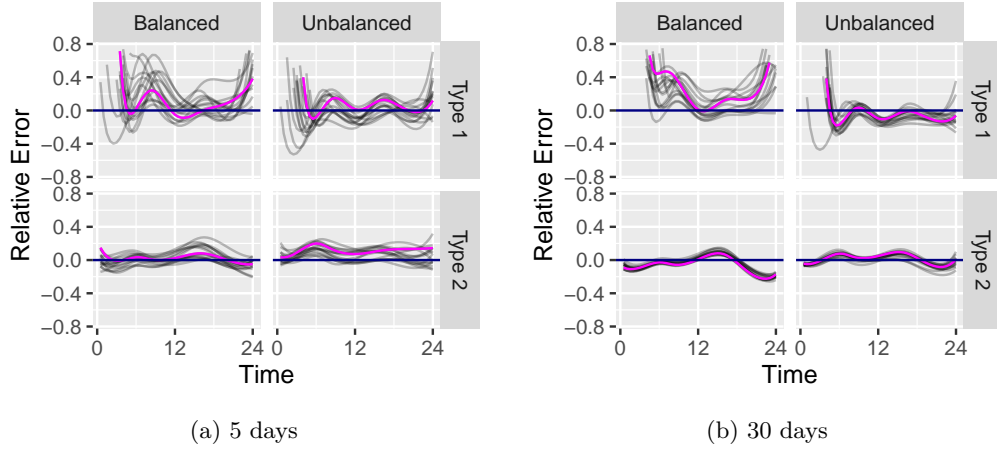


Figure 12: Residual curves of the estimated variance functionals for Scenarios 1 to 4 under the complete model fit. Median lines are represented in magenta and residual curves in gray.

1.3.3 Discussion and conclusion

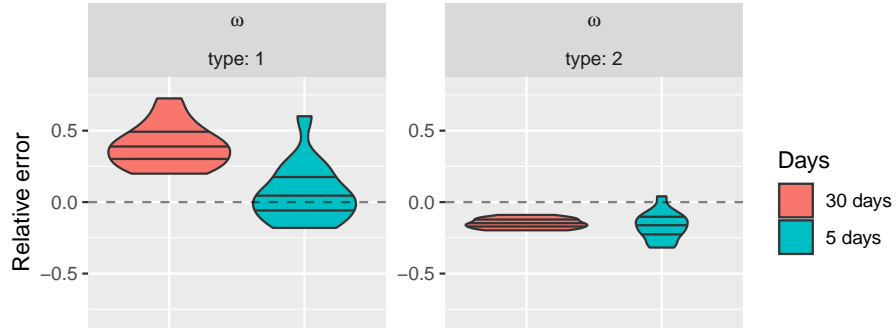
In all scenarios, the estimated typical surfaces of the homogeneous model are robust to the misspecification of the covariance structure, as shown in Figure 4. Both studies show an expected better performance for the 30-day scenarios in terms of estimation variability and fMSRE, which is also true for balanced scenarios compared to unbalanced ones.

Interestingly, it seems that the magnitude of the parameters may influence the quality of the estimate. The estimated typical curves, for example, show better estimates for customers of Type 2, the ones with higher consumption curves compared to Type 1. The same characteristic is observed in the relative errors of the estimates of γ_1 , a parameter much greater than γ_2 . Nonetheless, this is not as evident in the decay parameter estimation. The latter seems to be especially difficult to estimate because its performance in terms of precision and srMSRE (square root of the mean squared relative error) is not improved under 30-day scenarios or balanced markets. In fact, the estimates present a systematic underestimation of $\omega_2 = 0.70$. Still on the covariance structure, the estimated variance functionals in the complete study can capture the main features of the true ones, despite an unexpected local peak in the 30-day scenario with balanced market.

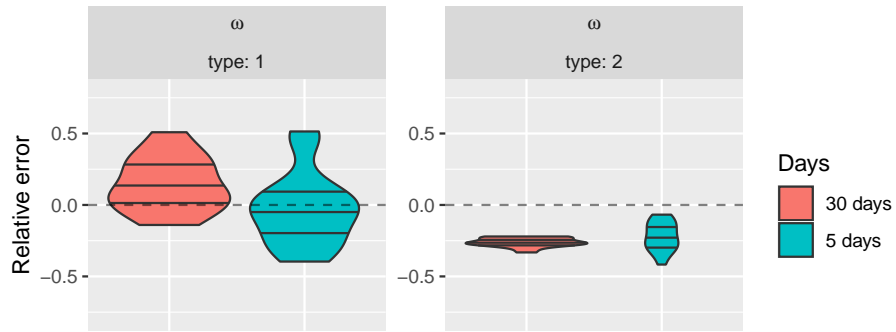
In general, the advantages of balanced markets and 30-day scenarios is evident. The complete model provides a functional variance structure that can capture different dispersions over time. However, in terms of typical surface estimation, there is no clear difference between the homogeneous and the complete model fit, which could be attributed to the fact that the least-squares estimators are unbiased independently of the covariance structure, as noted in Section 3.6 of the main text.

1.4 Clustering the aggregated model

This section studies the clustering approach of the aggregated data model presented in Section 3.5 of the main manuscript. The method was tested in Scenarios 5 to 8 and is presented in Table 2, where data from three clusters were simulated under the homogeneous covariance structure. In contrast to Section 1.3, typical surfaces were not considered here for the clustering model.



(a) Unbalanced market



(b) Balanced market

Figure 13: Relative errors of the estimated covariance parameters $\omega_1 = 0.03$ and $\omega_2 = 0.70$ for Scenarios 1 to 4, under the complete aggregated data model fit.

Section 1.4.1 details the clustering configuration and the true parameters. Sections 1.4.2 describes the main results and 1.4.3 contains the discussion and conclusions of this simulation study.

1.4.1 Clustering setup and true parameters

Scenarios 5 to 8 in Table 2 are made up of variations of the number of days (5 and 30) and the market (balanced and unbalanced). The remaining simulation parameters were fixed to three clusters and two types of customers observed in 12 substations every 30 minutes. The true cluster allocation is displayed in Table 6, where substations 1 to 6 are assigned to Cluster 1, substations 7 to 10 to Cluster 2 and finally substations 11 and 12 to Cluster 3. The chosen covariance structure is the homogeneous one, where each customer type has its own dispersion and decay parameters.

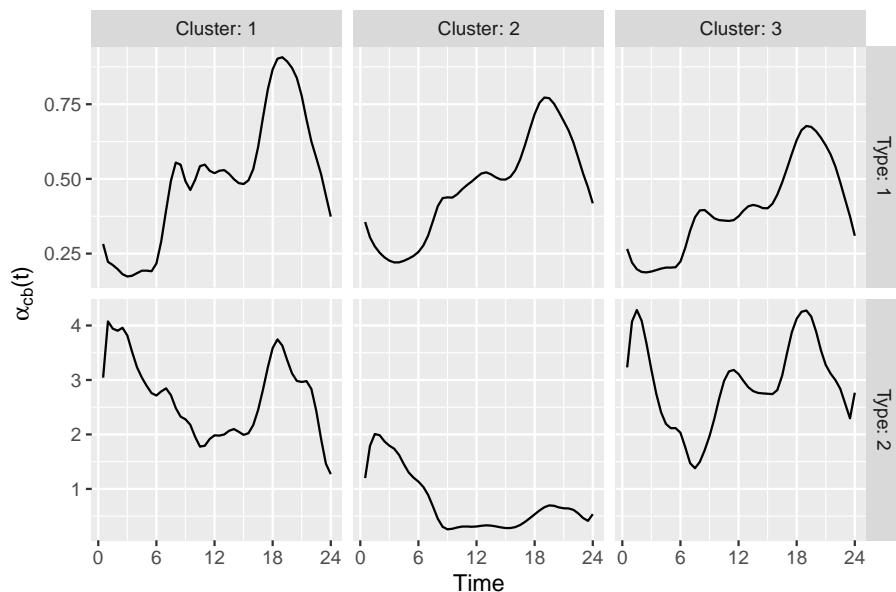


Figure 14: True typical curves for the clustering simulation considering three clusters and two customers types.

Figure 14 shows the six typical curves divided into the two customer types for each of the three clusters. Their shapes were based on the estimated typical curves for the UK energy grid dataset in Section 4.3 of the main paper. Hence, Type 1 mimics the unrestricted domestic customer, with similar shapes among clusters, whereas Type 2 mimics the “Economy 7” customer.

The covariance parameters that compose the homogeneous covariance structure of the simulated scenarios are presented in Table 7 divided by cluster, parameter and customer type, where, again, their values were based on the estimated covariance parameters for the UK energy grid dataset described in Section 4.3 of the main manuscript.

1.4.2 Results

Scenarios 5 to 8 were subjected to two model fits: clustering homogeneous aggregated data models with two and three clusters. The two-cluster fit tested how the model would perform if the number of clusters were underdetermined, that is, how the method groups substations and consequently what are the characteristics of the estimated typical curves and covariance parameters. On the other hand, the three-cluster fit evaluates model performance under correct scenarios.

Before presenting the results, it is necessary to note the number of runs that did not converge or converged to a local maximum in this simulation at each model fit. The non-convergent runs in the two-cluster fit were the following: two runs in the unbalanced five-day market scenario, one run in the balanced five-day market scenario, and two runs in the balanced 30-day market scenario. Moreover, the three-cluster fit had three non-convergent runs in both balanced and unbalanced five-day market scenarios, four in the unbalanced 30-day scenario, and two in the balanced 30-day scenarios. The runs that converged to local maxima presented anomalous estimated typical curves with negative and discrepant values.

Let us begin with the two-cluster fit and its respective substation clustering as shown in Table 8. In all runs, substations are assigned with high probability to the same cluster configuration, and therefore Substations 1 to 6 were assigned to Cluster 1, Substations 7 to 10 to Cluster 2, and Substations 11 and 12 to Cluster 3. Note that the substations of true Cluster 3 were assigned to the larger Cluster 1 in the two-cluster model. Recall also that the true Clusters 1 and 3 in Figure 14 have similar typical curves for Type 1 and Type 2 and that both have approximately the same magnitude and characteristics over time, and hence it is reasonable that they merge into a single cluster in the two-cluster model.

Figure 15 shows the estimated typical curves for Scenarios 5 to 8 under the two-cluster model fit. In general, observe that Cluster 1 curves capture the main characteristics of Clusters 1 and 3: the work period stability, the 8 PM peak of Type 1 curves, and the 2 AM and 8 PM peaks of Type 2 curves. The 30-day scenarios have slightly lower estimate variability than the five-day scenarios, but note that the Type 2 curves in Cluster 1 have runs with different estimated characteristics of the work period, as shown in Figures 15c and 15d. In fact, the main difference between true Clusters 1 and 3 is the work period characterization of Type 2, and therefore it is to be expected that some runs could estimate typical curves in favour of the true Cluster 1 or Cluster 3.

Table 9 shows the summary statistics of the estimated covariance parameters of the two-cluster model fit. Because the estimated Cluster 2 substations coincide with the substations in the true Cluster 2, it is to be expected that their estimated covariance parameters are close to their true values. Observe in Table 9 that the median and mean of the estimated parameters for Cluster 2 are close to their true values in the Reference column, especially for 30-day scenarios. Under five-day scenarios, balanced markets have better estimates in terms of precision. On the other hand, Cluster 1 estimates are located between the true values of true Clusters 1 and 3, and therefore the Reference column for Cluster 1 in Table 9 represents the mean of the covariance parameters of the true Clusters 1 and 3. The proximity of estimated and true covariance parameters is greater for customers of Type 2. In contrast, the Type 2 true dispersion parameters of Clusters 1 and 3 present the largest difference in Table 7, 1.54 and 5.18 respectively. Nonetheless, there is no clear evidence that the estimated covariance parameters in Cluster 1 are close to the average of the true parameters of Clusters 1 and 3.

The estimated typical curves of the three-cluster model are displayed in Figure 16 and their associated residual curves in Figure 17. In general, the median curves show that the estimated curves capture the main characteristics of the true typical curves, although there are visible

discrepant examples, more frequently seen in the unbalanced scenarios, as shown in Figures 16b and 16c. Negative values could be avoided by restricting the typical curve estimation, but to avoid overextending the computational burden of this simulation, it was decided to retain the least-squares estimators in exchange for some negative values, and also to show that in general the estimator is robust for different scenarios because the median curves are positive along the entire time axis. Once more, the residual curves show that the 30-day scenarios are more concentrated around the zero-reference line than the five-day scenarios, with even better fits for balanced scenarios. In this clustering approach, the relative residual curves for Cluster 3 in the unbalanced scenario do not concentrate around the zero-reference line, as shown in Figures 17b and 17d. Furthermore, Cluster 1 has residual curves with lower variability than Cluster 3 in all scenarios. In fact, Cluster 1 contains six substations, whereas Cluster 3 contains two substations, the minimum number required for model identifiability. It seems that the larger the number of substations in the cluster, the better is the precision, and consequently this might be the reason for the Cluster 3 overestimation of the typical curves, particularly under unbalanced scenarios.

The estimated covariance parameters of the three-cluster models are represented by their mean, median and srMSRE in Table 10. As observed in previous results throughout this section, smallest srMSRE are associated with parameters with larger magnitudes, for example, $\sigma_{22} = 1.28$ and $\sigma_{23} = 5.18$. In contrast, the largest srMSRE are associated with parameters with smaller magnitudes, for example, $\omega_{13} = 0.02$. In the latter case, the unbalanced scenarios presented smaller srMSRE than the balanced markets. In cases like $\omega_{22} = 0.09$, increasing the number of observation days from 5 to 30 improved srMSRE. The same behaviour was observed in most parameters, particularly those with small magnitude. On the other hand, parameters $\omega_{21} = 0.03$ and $\omega_{13} = 0.02$ were the smallest parameters in the simulation, but the srMSREs of ω_{21} were mostly around 1.5, whereas the srMSREs of ω_{13} had three values greater than 10. Recall that Cluster 3 contained only two substations. Therefore, as mentioned earlier for typical curve estimation, both the number of substations and the number of observation days are important to improve parameter estimation in each cluster.

To avoid an overextended table in this section, the comparison of BIC values between the two- and three-cluster models is presented in Table 12 in Section 1.5. In all cases, the BIC is favourable to the three-cluster model with differences mostly of order 10^2 .

Table 10: Mean, median and square root of the Mean Squared Relative Error (srMSRE) of the estimated covariance parameters for Scenarios 5 to 8, under the three-cluster model fit.

Parameter	Days	Market	Median	Mean	\sqrt{MSRE}
$\sigma_{11} = 1.54$	30 days	Balanced	1.0862	1.0114	0.6470
		Unbalanced	1.3929	1.2079	0.4677
	5 days	Balanced	0.9430	0.8281	0.6991
		Unbalanced	1.3859	1.2022	0.4923
$\omega_{11} = 0.16$	30 days	Balanced	0.3220	2.2018	3.5878
		Unbalanced	0.1295	0.3441	1.1971
	5 days	Balanced	3.9317	6.5328	6.3132
		Unbalanced	0.1274	0.9780	2.3491
	30 days	Balanced	2.8842	2.9041	0.9477
		Unbalanced	2.7891	2.8831	0.9404

Table 10 (continued)

Parameter	Days	Market	Median	Mean	\sqrt{MSRE}
$\sigma_{21} = 1.53$	5 days	Balanced	2.8640	2.9372	0.9590
		Unbalanced	2.7464	2.7632	0.9386
$\omega_{21} = 0.03$	30 days	Balanced	0.0759	0.0777	1.2608
		Unbalanced	0.0960	0.0985	1.5111
	5 days	Balanced	0.0736	0.0807	1.3000
		Unbalanced	0.1057	0.4043	3.5322
$\sigma_{12} = 1.07$	30 days	Balanced	1.0274	1.0346	0.4578
		Unbalanced	1.0810	1.1472	0.3197
	5 days	Balanced	0.6081	0.6888	0.7774
		Unbalanced	1.2345	1.2259	0.4379
$\omega_{12} = 0.12$	30 days	Balanced	0.1208	0.6763	2.1698
		Unbalanced	0.1226	0.1344	0.4184
	5 days	Balanced	1.4476	2.4465	4.4133
		Unbalanced	0.1083	0.5807	2.0123
$\sigma_{22} = 1.28$	30 days	Balanced	1.5417	1.5858	0.4888
		Unbalanced	1.2823	1.2391	0.4312
	5 days	Balanced	1.5092	1.5814	0.4852
		Unbalanced	0.0363	0.5207	0.9565
$\omega_{22} = 0.09$	30 days	Balanced	0.0960	0.0965	0.2692
		Unbalanced	0.1057	0.4156	1.9330
	5 days	Balanced	0.0877	0.0884	0.2444
		Unbalanced	5.2492	5.6967	7.8929
$\sigma_{13} = 0.43$	30 days	Balanced	0.3390	1.4096	1.7326
		Unbalanced	1.3438	1.4685	1.5540
	5 days	Balanced	0.0282	0.4760	1.1353
		Unbalanced	1.0871	1.0075	1.3569
$\omega_{13} = 0.02$	30 days	Balanced	3.9775	3.2759	12.7591
		Unbalanced	0.1446	0.3754	4.2157
	5 days	Balanced	9.9767	10.3302	22.7049
		Unbalanced	0.9252	2.7126	11.6030
$\sigma_{23} = 5.18$	30 days	Balanced	5.2455	5.0097	0.3249
		Unbalanced	3.9596	3.3274	0.5980
	5 days	Balanced	4.7792	4.6787	0.3502
		Unbalanced	4.0859	3.9616	0.4917
	30 days	Balanced	0.2624	0.2492	0.5713
		Unbalanced	0.2968	0.6871	1.1099

Table 10 (continued)

Parameter	Days	Market	Median	Mean	\sqrt{MSRE}
$\omega_{23} = 0.37$	5 days	Balanced	0.1930	0.1960	0.6859
		Unbalanced	0.2759	0.8170	1.3016

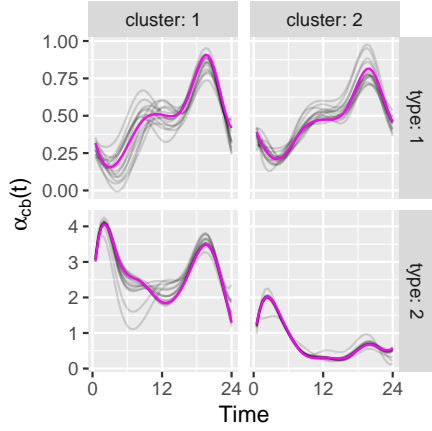
1.4.3 Discussion and conclusion

In both fitted models, substations are allocated to the same clusters throughout the series of runs. In the two-cluster model, Substations 11 and 12, which belong to the true Cluster 3, are always assigned to Cluster 1 together with Substations 1 to 6. In this case, with an underdetermined number of clusters, the method groups the clusters with more similarity. Hence the estimated typical curves for Cluster 1 still capture the main features of the true curves for Clusters 1 and 3. Similarly, the estimated covariance parameters for Cluster 1 present values between the true covariance parameters of the true Clusters 1 and 3. In the three-cluster model, substations are assigned to the correct cluster. Consequently, except for some cases under unbalanced scenarios, estimated typical curves for this model are well located around their true curves. In general, 30-day scenarios have less dispersed estimates than five-day scenarios, and balanced markets have less dispersed estimates than unbalanced ones.

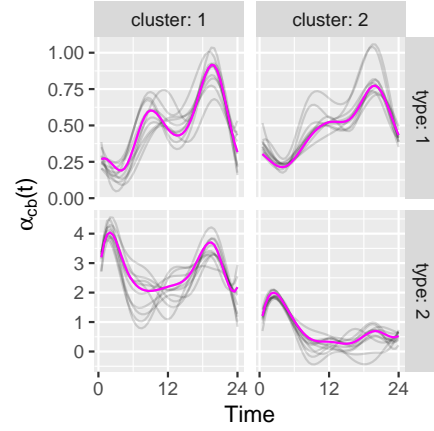
The differences among scenarios have a similar impact on the estimation of covariance parameters. In addition, there is evidence that the number of substations in a cluster is crucial to estimation performance, particularly for small-magnitude parameters. The positive impact of increasing the number of substations on parameter estimation is shown in Lenzi et al. [2017]. Two parameters with small values for Clusters 1 and 3 have distinct srMSRE probably because the information available for Cluster 3 estimation is less than for Cluster 1.

When comparing both models, the three-cluster model presents lower BIC than the two-cluster model in all cases. In a real-world problem, where the true number of clusters is unknown, the BIC can be a useful tool to decide between models.

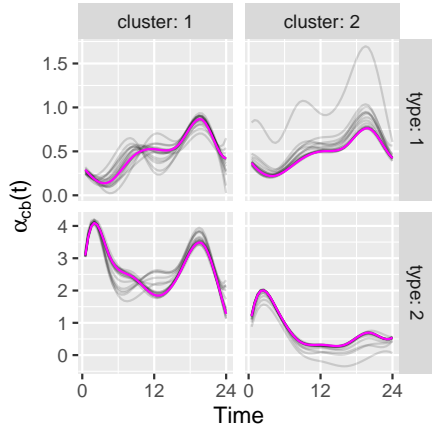
Users of the clustering aggregated data model are encouraged to be careful with the estimated covariance parameters and to try multiple models with different numbers of clusters using these estimated values as input for their initial values. For example, the estimated values of the aggregated two-cluster data model can be used as an input to fit the aggregated three-cluster data model by repeating one of the results. As shown in Section 2.5, after multiple fits, the user can compare the models using the likelihood test ratio to help decide which model is the most adequate to the data.



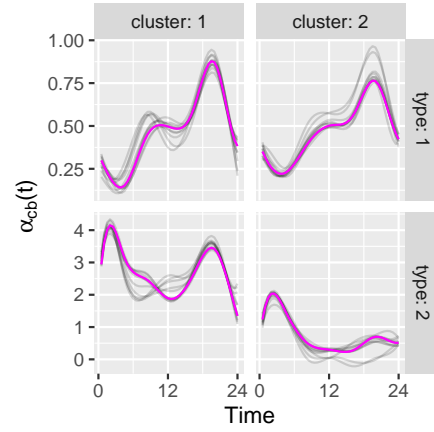
(a) Balanced market with 5-day data



(b) Unbalanced market with 5-day data

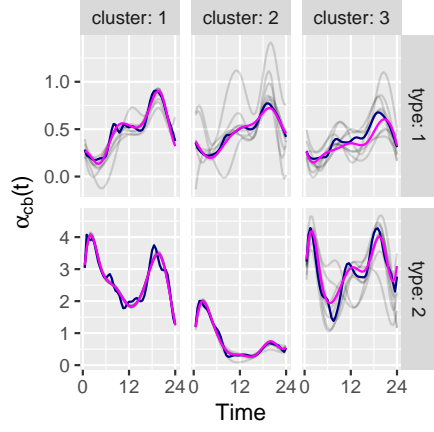


(c) Balanced market with 30-day data

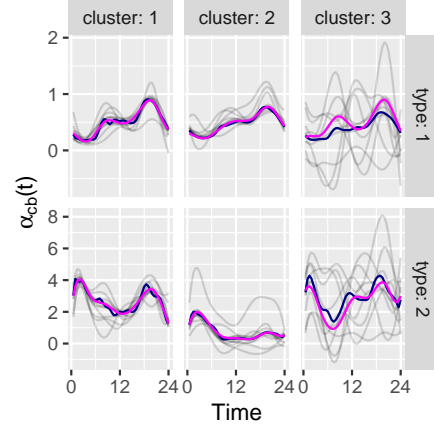


(d) Unbalanced market with 30-day data

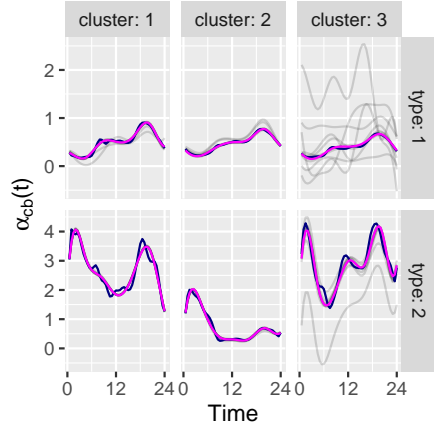
Figure 15: Estimated typical curves for Scenarios 5 to 8, represented by the combination of market balance and number of days, under the two-cluster model. Median curves are represented in magenta and estimated typical curves in gray.



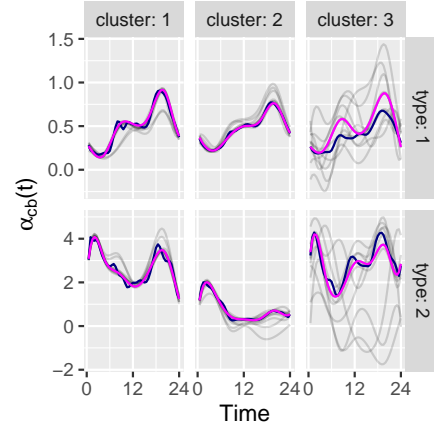
(a) Balanced market with 5-day data



(b) Unbalanced market with 5-day data

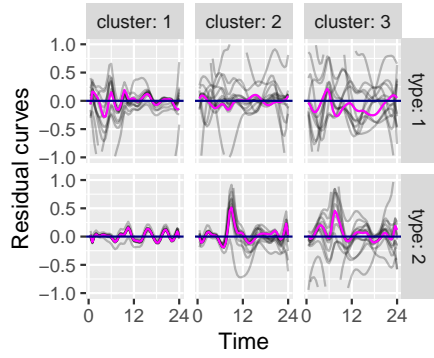


(c) Balanced market with 30-day data

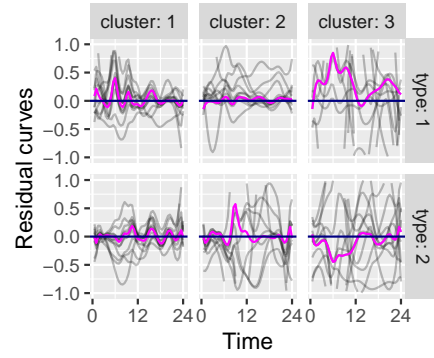


(d) Unbalanced market with 30-day data

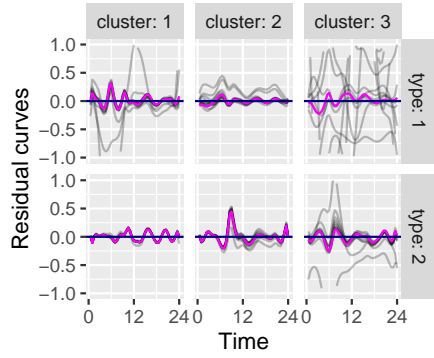
Figure 16: Estimated typical curves for Scenarios 5 to 8, represented by the combination of market balance and number of days, under the three-cluster model. Median curves are represented in magenta and estimated typical curves in gray.



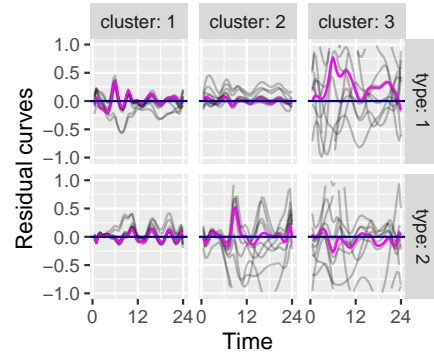
(a) Balanced market with 5-day data



(b) Unbalanced market with 5-day data



(c) Balanced market with 30-day data



(d) Unbalanced market with 30-day data

Figure 17: Residual curves for Scenarios 5 to 8, represented by the combination of market balance and number of days, under the three-cluster model. Median curves are represented in magenta and estimated typical curves in gray..

Table 4: Mean, median and square root of the Mean Squared Relative Error (MSRE) of the estimated explanatory variables parameters under the homogeneous and complete model fit for Scenarios 1 to 4.

Model	Parameter	Days	Market	Mean	Median	\sqrt{MSRE}
Homogeneous	$\gamma_1 = 13$	30 days	Balanced	12.7193	12.0985	0.3054
			Unbalanced	11.8776	12.1702	0.2516
		5 days	Balanced	12.0501	12.1832	1.7045
			Unbalanced	17.2909	8.3669	1.6263
	$\gamma_2 = 0.0011$	30 days	Balanced	0.0330	0.0421	3.4016
			Unbalanced	0.0289	0.0328	2.9574
		5 days	Balanced	0.0156	-0.0159	14.6551
			Unbalanced	0.0231	0.0334	5.6259
Complete	$\gamma_1 = 13$	30 days	Balanced	13.3503	12.9929	0.2578
			Unbalanced	11.8177	12.1773	0.2295
		5 days	Balanced	11.3529	15.1660	1.6096
			Unbalanced	15.3926	9.1294	1.1091
	$\gamma_2 = 0.0011$	30 days	Balanced	0.0330	0.0490	3.0979
			Unbalanced	0.0283	0.0337	2.5957
		5 days	Balanced	0.0254	0.0104	15.3070
			Unbalanced	0.0274	0.0264	5.4715

Table 5: Mean, median and square root of the Mean Squared Relative Error (MSRE) of the estimated decay parameters for Scenarios 1 to 4, under the homogeneous model fit.

Model	Parameter	Days	Market	Median	Mean	\sqrt{MSRE}
Homogeneous	$\omega_1 = 0.03$	30 days	Balanced	0.0257	0.0275	0.2549
			Unbalanced	0.0382	0.0322	0.5544
		5 days	Balanced	0.0270	0.0259	0.2107
			Unbalanced	0.0287	0.0764	6.6934
	$\omega_2 = 0.70$	30 days	Balanced	0.5028	0.5079	0.2764
			Unbalanced	0.5520	0.5562	0.2111
		5 days	Balanced	0.5226	0.5251	0.2675
			Unbalanced	0.5427	0.5073	0.3318
Complete	$\omega_1 = 0.03$	30 days	Balanced	0.0316	0.0298	0.4243
			Unbalanced	0.0419	0.0418	0.4208
		5 days	Balanced	0.0288	0.0291	0.2516
			Unbalanced	0.0312	0.0318	0.2065
	$\omega_2 = 0.70$	30 days	Balanced	0.5169	0.5178	0.2621
			Unbalanced	0.5899	0.5962	0.1521
		5 days	Balanced	0.5323	0.5450	0.2418
			Unbalanced	0.5819	0.5831	0.1917

Table 6: True cluster assignment for each substation in the simulation study.

Substation	1	2	3	4	5	6	7	8	9	10	11	12
True cluster	1	1	1	1	1	1	2	2	2	2	3	3

Table 7: True covariance parameters for clustering simulation considering three clusters and two customer types.

Cluster	Parameter	Type	Value
$b = 1$	σ_{cb}	$c = 1$	1.54
		$c = 2$	1.53
	ω_{cb}	$c = 1$	0.16
		$c = 2$	0.03
$b = 2$	σ_{cb}	$c = 1$	1.07
		$c = 2$	1.28
	ω_{cb}	$c = 1$	0.12
		$c = 2$	0.09
$b = 3$	σ_{cb}	$c = 1$	0.43
		$c = 2$	5.18
	ω_{cb}	$c = 1$	0.02
		$c = 2$	0.37

Table 8: Cluster allocation of the 12 substations under the clustering models with two and three clusters. The proportion of runs assigned to that cluster are 100% in all runs in both model fit.

Substation	True	two-cluster fit	three-cluster fit
1	1	1	1
2	1	1	1
3	1	1	1
4	1	1	1
5	1	1	1
6	1	1	1
7	2	2	2
8	2	2	2
9	2	2	2
10	2	2	2
11	3	1	3
12	3	1	3

Table 9: Summary statistics for the estimated covariance parameters for Scenarios 5 to 8 under the two-cluster model fit. The reference column for Cluster 1 (parameter subindex ending in 1) is the mean value between covariance parameters of the true Clusters 1 and 3 and for Cluster 2 (parameter subindex ending in 2) is the true covariance parameters for the true Cluster 2.

Parameter	Days	Market	Ref	Median	Mean	Std Dev
σ_{11}	30 days	Balanced	0.985	1.3690	1.1717	0.6952
		Unbalanced	0.985	1.4175	1.4324	0.1123
	5 days	Balanced	0.985	1.2360	1.0226	0.5916
		Unbalanced	0.985	1.3903	0.9552	0.7257
ω_{11}	30 days	Balanced	0.090	0.1863	1.7907	3.2170
		Unbalanced	0.090	0.1303	0.1457	0.0323
	5 days	Balanced	0.090	0.2262	2.4892	3.6509
		Unbalanced	0.090	0.4885	1.7235	2.2490
σ_{21}	30 days	Balanced	3.355	3.3149	3.7087	1.0352
		Unbalanced	3.355	3.8129	3.3212	0.7789
	5 days	Balanced	3.355	4.0515	4.0523	0.7751
		Unbalanced	3.355	3.7831	4.1194	0.9537
ω_{21}	30 days	Balanced	0.200	0.1247	0.1559	0.0653
		Unbalanced	0.200	0.1859	0.1728	0.0768
	5 days	Balanced	0.200	0.1983	0.1848	0.0644
		Unbalanced	0.200	0.2595	0.2048	0.0891
σ_{12}	30 days	Balanced	1.070	1.1663	1.2281	0.3476
		Unbalanced	1.070	1.0870	1.1621	0.1524
	5 days	Balanced	1.070	1.0906	1.1274	0.3569
		Unbalanced	1.070	1.2591	1.1776	0.3398
ω_{12}	30 days	Balanced	0.120	0.1290	0.3108	0.7708
		Unbalanced	0.120	0.1143	0.1152	0.0071
	5 days	Balanced	0.120	0.1080	0.3592	1.0368
		Unbalanced	0.120	0.1134	1.0093	2.3378
σ_{22}	30 days	Balanced	1.280	1.4533	1.3147	0.3727
		Unbalanced	1.280	1.3541	1.2999	0.8166
	5 days	Balanced	1.280	1.4583	0.9738	0.7445
		Unbalanced	1.280	0.3949	0.8713	1.0385
ω_{22}	30 days	Balanced	0.090	0.0958	0.3894	0.8949
		Unbalanced	0.090	0.1233	1.4038	2.7188
	5 days	Balanced	0.090	0.0998	2.2790	3.1786
		Unbalanced	0.090	3.6099	4.7933	4.9760

1.5 Additional tables

Table 11: Likelihood ratio test comparison table of homogeneous and complete aggregated data models in simulated datasets for each experimental run. The degrees of freedom used to compute the p-value is 10 for all comparisons.

Days	Run	Log-likelihood		Test statistic	p-value
		Homogeneous	Complete		
5 days	1	11356.44	11206.11	300.6677	<0.0001
5 days	2	11468.83	11279.91	377.8489	<0.0001
5 days	3	11329.26	11129.60	399.3154	<0.0001
5 days	4	11393.79	11237.21	313.1679	<0.0001
5 days	5	11380.05	11161.95	436.2019	<0.0001
5 days	6	11412.08	11240.27	343.6055	<0.0001
5 days	7	11409.96	11230.16	359.5910	<0.0001
5 days	8	11380.91	11221.02	319.7964	<0.0001
5 days	9	11296.43	11111.48	369.8967	<0.0001
5 days	10	11293.50	11131.60	323.7867	<0.0001
5 days	11	11297.66	11132.56	330.1824	<0.0001
5 days	12	11380.86	11204.74	352.2391	<0.0001
5 days	13	11305.42	11135.14	340.5573	<0.0001
5 days	14	11357.41	11182.27	350.2775	<0.0001
5 days	15	11337.32	11153.20	368.2447	<0.0001
5 days	16	12252.88	12167.35	171.0486	<0.0001
5 days	17	12199.07	12079.56	239.0298	<0.0001
5 days	18	12315.08	12222.54	185.0706	<0.0001
5 days	19	12394.19	12316.81	154.7764	<0.0001
5 days	20	12254.24	12160.62	187.2429	<0.0001
5 days	21	12286.01	12189.36	193.3048	<0.0001
5 days	22	12314.49	12225.54	177.8949	<0.0001
5 days	23	12173.57	12073.10	200.9313	<0.0001
5 days	24	12248.57	12150.72	195.6961	<0.0001
5 days	25	12197.71	12090.13	215.1580	<0.0001
5 days	26	12304.61	12196.86	215.4922	<0.0001
5 days	27	12135.35	12034.37	201.9598	<0.0001
5 days	28	12385.44	12302.31	166.2589	<0.0001
5 days	29	12359.07	12253.33	211.4677	<0.0001
5 days	30	12249.15	12142.30	213.7031	<0.0001
30 days	1	68412.15	67418.28	1987.7512	<0.0001
30 days	2	68555.41	67692.07	1726.6639	<0.0001
30 days	3	68409.85	67507.56	1804.5693	<0.0001
30 days	4	68848.74	67854.20	1989.0811	<0.0001
30 days	5	68853.23	67912.53	1881.3950	<0.0001

30 days	6	68254.05	67181.14	2145.8196	<0.0001
30 days	7	68428.22	67442.46	1971.5111	<0.0001
30 days	8	68720.86	67794.68	1852.3555	<0.0001
30 days	9	68143.11	67241.85	1802.5107	<0.0001
30 days	10	68639.51	67645.38	1988.2693	<0.0001
30 days	11	68532.07	67568.32	1927.5025	<0.0001
30 days	12	68452.58	67430.66	2043.8409	<0.0001
30 days	13	68697.84	67687.06	2021.5609	<0.0001
30 days	14	68183.63	67221.51	1924.2479	<0.0001
30 days	15	68828.41	67972.03	1712.7790	<0.0001
30 days	16	73834.91	73325.45	1018.9162	<0.0001
30 days	17	74309.19	73894.94	828.4990	<0.0001
30 days	18	74396.67	73964.25	864.8214	<0.0001
30 days	19	74607.51	74136.77	941.4789	<0.0001
30 days	20	74741.17	74284.07	914.1883	<0.0001
30 days	21	74686.06	74273.96	824.1941	<0.0001
30 days	22	74678.44	74242.28	872.3236	<0.0001
30 days	23	74295.85	73798.20	995.2966	<0.0001
30 days	24	73439.84	72817.88	1243.9196	<0.0001
30 days	25	74510.71	74113.48	794.4602	<0.0001
30 days	26	74232.01	73790.03	883.9603	<0.0001
30 days	27	74783.54	74378.31	810.4463	<0.0001
30 days	28	74510.23	74068.60	883.2588	<0.0001
30 days	29	74963.07	74588.12	749.8957	<0.0001
30 days	30	74913.23	74506.08	814.3098	<0.0001

Table 12: BIC values for the clustering aggregated data models in simulated datasets at each experimental runs. NA values represent the runs that did not converge.

Days	Run	BIC		BIC diff
		2 Clusters	3 Clusters	
5 days	1	22892.98	22653.75	239.24
5 days	2	23037.71	22728.32	309.38
5 days	3	22765.23	22522.55	242.68
5 days	4	23002.98	22632.54	370.44
5 days	5	NA	NA	NA
5 days	6	22867.82	22589.01	278.82
5 days	7	22928.48	22674.78	253.70
5 days	8	23057.19	NA	NA
5 days	9	23110.73	22797.53	313.20
5 days	10	NA	NA	NA
5 days	11	23023.11	22788.12	234.99
5 days	12	22893.37	22633.57	259.80
5 days	13	23033.60	22798.68	234.93
5 days	14	22996.42	22713.55	282.87
5 days	15	23127.33	22832.22	295.11
5 days	16	24320.71	23984.69	336.02
5 days	17	24930.08	24283.66	646.42
5 days	18	24508.43	NA	NA
5 days	19	24306.36	24053.74	252.62
5 days	20	24582.05	24364.63	217.42
5 days	21	24138.96	23911.80	227.16
5 days	22	24580.06	24236.24	343.83
5 days	23	24477.64	NA	NA
5 days	24	24365.16	24106.78	258.37
5 days	25	NA	NA	NA
5 days	26	24842.38	24266.45	575.93
5 days	27	23893.08	23763.69	129.38
5 days	28	24568.87	24068.67	500.20
5 days	29	24718.34	24275.80	442.54
5 days	30	24304.65	24030.62	274.03
30 days	1	140732.75	139731.99	1000.75
30 days	2	137862.55	137674.83	187.73
30 days	3	141129.86	140153.32	976.53
30 days	4	139429.37	NA	NA
30 days	5	138120.81	137360.21	760.60
30 days	6	138909.99	NA	NA
30 days	7	138244.85	NA	NA

30 days	8	139216.20	138601.06	615.15
30 days	9	138597.82	137882.19	715.63
30 days	10	137915.18	NA	NA
30 days	11	139329.72	138463.56	866.16
30 days	12	138265.27	NA	NA
30 days	13	139177.05	138376.03	801.02
30 days	14	137716.41	136986.04	730.38
30 days	15	138839.29	138544.00	295.30
30 days	16	148793.81	NA	NA
30 days	17	151598.28	149765.27	1833.01
30 days	18	148195.67	146904.43	1291.24
30 days	19	146444.55	145965.37	479.17
30 days	20	150741.62	148847.58	1894.04
30 days	21	145479.22	144462.94	1016.28
30 days	22	147632.69	146775.49	857.20
30 days	23	149746.58	148789.10	957.48
30 days	24	NA	148840.17	NA
30 days	25	151627.47	150116.68	1510.80
30 days	26	NA	150376.76	NA
30 days	27	150394.95	NA	NA
30 days	28	149657.30	147460.43	2196.86
30 days	29	147228.13	146344.21	883.91
30 days	30	152994.93	150468.24	2526.69

References

Amanda Lenzi, Camila P. E. de Souza, Ronaldo Dias, Nancy L. Garcia, and Nancy E. Heckman. Analysis of aggregated functional data from mixed populations with application to energy consumption. *Environmetrics*, 28(2):e2414, 2017.